


RESEARCH ARTICLE

Open Access



Sedimentary diversity of the 2011 Tohoku-oki tsunami deposits on the Sendai coastal plain and the northern coast of Fukushima Prefecture, Japan

Dan Matsumoto^{1*} , Yuki Sawai¹, Koichiro Tanigawa¹, Yuichi Namegaya¹, Masanobu Shishikura¹, Kyoko Kagohara², Osamu Fujiwara¹ and Tetsuya Shinozaki^{1,3}

Abstract

This paper documents the sedimentary characteristics of the widespread deposits associated with the 2011 Tohoku-oki tsunami on the lowlands along the Pacific coast of the Sendai and Fukushima regions, northern Japan, and observed tsunami inundation depths. In eight areas of the region, field observation was carried out at a total of 123 locations and sampling at a total of 49 locations. Grain-size analysis and soft X-ray imaging reveal that the tsunami deposits are usually composed of sheetlike sandy beds and generally show landward-thinning and landward-fining trends and a landward increase in mud content, although site-specific distributional patterns are apparent along each transect. These thickness and grain-size patterns indicate a landward decrease in flow capacity. This information on the sedimentology of tsunami deposits and observed inundation depths will assist with the identification of paleo-tsunami deposits in the geological record and provide valuable constraints for mathematical analyses of tsunami hydraulic conditions related to sedimentary characteristics.

Keywords 2011 Tohoku-oki tsunami, Tsunami deposit, Sedimentary structures, Grain size, Thickness

1 Introduction

Tsunami deposits are reliable evidence for recent, historical, and prehistoric tsunamis and can be exploited to reconstruct tsunami recurrence intervals by dating (Nanayama *et al.* 2003; Cisternas *et al.* 2005; Kelsey *et al.* 2005; Jankaew *et al.* 2008; Sawai *et al.* 2009b; Dura *et al.* 2017; Ishizawa *et al.* 2017, 2019; Rubin *et al.* 2017;

Fujino *et al.* 2018; Shimada *et al.* 2019; Higaki *et al.* 2021), tsunami inundation areas on the basis of their spatial distributions (MacInnes *et al.* 2010; Sawai *et al.* 2012, 2015; Sugawara *et al.* 2013; Pilarczyk *et al.* 2021), and the hydraulic conditions of tsunamis by inverse modeling (Jaffe and Gelfenbaum 2007; Jaffe *et al.* 2012; Goto *et al.* 2014; Naruse and Abe 2017; Tang and Weiss 2015; Tang *et al.* 2017; Mitra *et al.* 2020, 2021). In general, tsunami deposits are initially identified as coarse layers within fine strata by visual observation and soft X-ray imaging and are then diagnosed using multiple approaches (e.g., sedimentological, paleontological, and/or geochemical analyses; Goff *et al.* 2012). To eliminate other possibilities for the origins of the coarse-grained event deposits, such as river flooding and storm surge events (e.g., Tuttle *et al.* 2004; Morton *et al.* 2007), a comparison of paleo- and modern tsunami deposits is essential.

*Correspondence:

Dan Matsumoto
dan-matsumoto@aist.go.jp

¹ Geological Survey of Japan, National Institute of Advanced Industrial Science and Technology (AIST), Tsukuba Central 7, 1-1-1 Higashi, Tsukuba, Ibaraki 305-8567, Japan

² Department of Social Studies, Faculty of Education, Yamaguchi University, 1677-1 Yoshida, Yamaguchi, Yamaguchi 753-8513, Japan

³ Present Address: National Museum of Japanese History, 117 Jonai-cho, Sakura, Chiba 285-8502, Japan

The tsunami deposits associated with the 2011 Tohoku-oki tsunami have been well documented (e.g., Goto et al. 2011, 2012, 2014; Abe et al. 2012, 2020; Chagué-Goff et al. 2012a, b; Jaffe et al. 2012; Naruse et al. 2012; Szczuciński et al. 2012; Pilarczyk et al. 2012; Richmond et al. 2012; Takashimizu et al. 2012; Matsumoto et al. 2016; Tanigawa et al. 2018; Iijima et al. 2021). For example, Goto et al. (2011) and Abe et al. (2012) observed sandy and muddy tsunami deposits on the Sendai Plain and compared their distributions to the area inundated by seawater during the tsunami event. Additionally, Goto et al. (2014) described changes in the thicknesses of the tsunami deposits from approximately 1300 locations, as well as flow-depth and elevation data on the Sendai Plain, to investigate the relations between these parameters. Those reports provided valuable information on the 2011 tsunami deposits as modern analogs for identifying paleo-tsunami deposits; however, detailed descriptions of sedimentary features and grain-size data in each location have not yet been published. Thus, although the 2011 tsunami provided considerable knowledge and abundant data on tsunami deposits have been obtained in previous studies, these data are uneven in their spatial and vertical resolution.

In this paper, we provide archives of visual images including soft X-ray images and thickness and grain-size data for the 2011 Tohoku-oki tsunami deposits, allowing direct comparison between the various locations and areas. The archives of the tsunami deposits were obtained from the Sendai Plain and the Fukushima coast, which were little investigated immediately after the tsunami, to document their sedimentological features. We also provide thickness and grain-size data at 1-cm vertical intervals along leveled transects. This unparalleled dataset will serve as an archive that will improve the identification of paleo-tsunami deposits and enable precise estimates of the hydraulic conditions of inundation flow via inverse modeling.

2 Study area

2.1 Geomorphological setting

Our field investigations were conducted along an approximately 80-km north–south distance along the coasts of the Sendai Plain and the northern part of Fukushima Prefecture (Fig. 1). We considered eight study areas that extend up to 5 km inland (Fig. 1B), which are, from north to south, the Onuma, Arahama, Natori, Watari, Yamamoto, Suijin-numa, Shinchi, and Odaka areas (Fig. 1B). The first five areas are located on the Sendai Plain, which extends about 50 km from north to south. The Sendai Plain is approximately 10 km wide in its northern part around the Onuma and Arahama areas, and narrows toward the south to less than 5 km wide around the

Yamamoto area (Fig. 1). The Sendai Plain is a flat lowland, generally has an elevation above sea level of less than 5 m, and is characterized by beach ridges and muddy inter-ridge swales (now used as paddy fields) that lie parallel to the coastline (Tamura and Masuda 2004). The average gradient is gentle within the study areas in the Sendai Plain: about 0.3‰ in the Natori area, 0.4–0.5‰ in the Onuma, Arahama, and Watari areas; and 0.8‰ in the Yamamoto area. The three southernmost study areas are located on lowlands in narrow valleys between the hills (known as the Soso Hills, Fukushima Prefecture), which are up to several tens of meters high. These lowlands are generally at less than 5 m elevation, and each has a narrow (maximum 1 km wide) eastward opening and extends 2–4 km in the east–west direction. The average gradient is relatively high in these three areas: about 3‰ in the Suijin-numa area; 2‰ in the Shinchi area; and 1‰ in the Odaka area.

2.2 The 2011 Tohoku-oki tsunami in the study area

Field surveys of inundation depths, heights, and areas associated with the 2011 tsunami in the study areas have been conducted by many researchers. Inundation depths above the surrounding ground levels in these areas were measured by using watermarks and calibrated to provide inundation heights relative to the mean sea level of Tokyo Bay (Tokyo Peil). These survey results were compiled by the joint survey group (The Tohoku Earthquake Tsunami Joint Survey Group 2011; Mori et al. 2012). The Geospatial Information Authority of Japan provided the inundation map, which was estimated from interpretations of aerial photographs and satellite images (Nakajima and Koarai 2011). The maximum inundation distance and inundation heights within each study area are summarized in Table 1. In addition, Goto et al. (2012) concluded that the first wave was the largest and reached the furthest inundation distance on the Sendai Plain.

3 Methods

We conducted field investigations in April and May 2011, January 2012, and November 2015 (Table 2). We selected a total of 123 study locations within the eight study areas: Onuma (ON1–17); Arahama (AR1–21); Natori (NT1–16); Watari (WT1–17); Yamamoto (YM1–27); Suijin-numa (SJ1–9); Shinchi (SN1–8); and Odaka (OD1–8) (Figs. 1, 2; Table 2). We excavated small pits, observed the grain size and sedimentary structures of the tsunami deposits, and measured their thicknesses at every study location (white and pink circles in Fig. 2), except for two locations (AR21 and OD8) at which no tsunami deposits, not even thin mud drapes, were found. We obtained samples of the tsunami deposits for laboratory analysis at 49 locations with a plate-shaped plastic case (pink circles

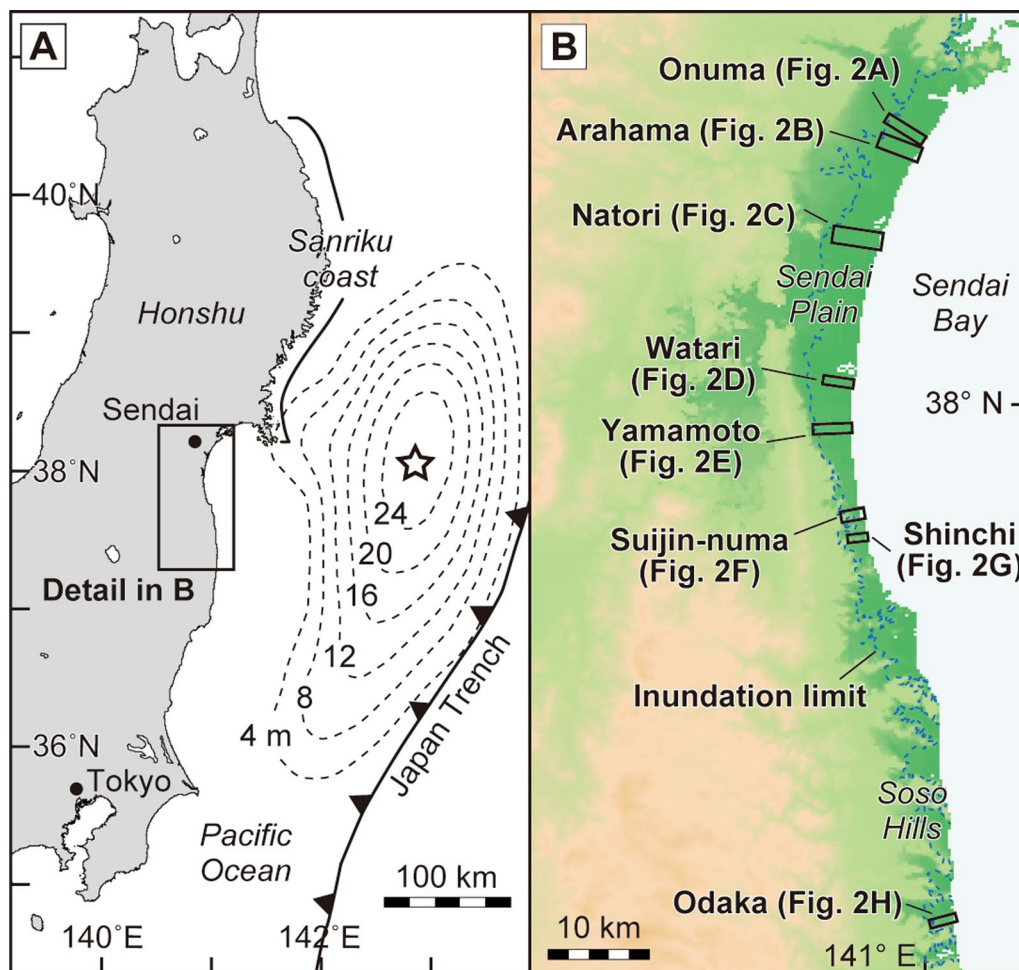


Fig. 1 Location map of study areas along the Pacific coast around the Tohoku district, northeastern Japan. **A** Index map of northeastern Japan showing the Pacific coast around the Tohoku district. The epicenter of the 2011 Tohoku-oki earthquake (star) and the coseismic slip distribution (dashed lines; Ozawa et al. 2011) are marked. **B** Detailed index map of the eight study areas along the Pacific coast. Study locations within each area are shown in Fig. 2. The inundation limit of the 2011 tsunami (dashed blue line) follows the “1:100,000 tsunami flood area overview map” on the GSI Web site (Nakajima and Koarai 2011)

Table 1 Summary of maximum inundation distances and heights within the studied areas

Area	Maximum inundation distance (km)	Maximum inundation height (m)
Onuma and Arahama	5.3	19.7
Natori	5.3	13.1
Watari	4.3	8.6
Yamamoto	3.5	10.3
Suijin-numa	2.1	13.5
Shinchi	2.2	8.7
Odaka	2.1	12.2

Maximum inundation distances are based on the “1:100,000 tsunami flood area overview map” on the GSI Web site (Nakajima and Koarai 2011), and heights are according to The Tohoku Earthquake Tsunami Joint Survey Group (2011) and Mori et al. (2012)

in Fig. 2). Inundation depths were measured using watermarks at seven locations within the study areas (blue squares in Fig. 2; Table 3). We also surveyed the topography along east–west transects within the Shinchi and Odaka areas using VRS-GNSS survey instruments (Viva GS10, Leica Geosystems AG, Heerbrugg, Switzerland) in November 2015 (Figs. 2G, H, 3).

In the laboratory, soft X-ray imaging was carried out on the samples from 49 locations (Table 2) with a soft X-ray apparatus (SOFRON SRO-i503-2, SOFTEX Co., Ltd., Tokyo, Japan) and a digital X-ray sensor (NAOMI NX-04SN, RF Co., Ltd., Nagano, Japan). Grain-size analyses of the samples were conducted using an image analyzer (Retsch Camsizer, Verder Scientific, Haan, Germany), which has a wide effective measuring range that can

Table 2 Survey locations, survey dates, and deposits in each area

Area	Location	GPS coordinates		Distance (m)	Thickness (cm)	Description	Tsunami deposit		Underlying soil		Overlying mud drape		Survey Date
		Latitude	Longitude				Mean grain size (phi)	Mud content (%)	Mean grain-size (phi)	Mud content (%)	Mean grain-size (phi)	Mud content (%)	
Onuma	ON1	38.228889	140.982611	918	13	Lower c. sand and upper vf. sand layers including mud clast at the bottom and muddy thin layer at the middle with a mud drape	Mean grain size (phi)	Mud content (%)	Mean grain-size (phi)	Mud content (%)	Mean grain-size (phi)	Mud content (%)	May 2011
	ON2	38.229500	140.981556	1042	14	Lower m.-c. sand and upper vf.-f. sand layers including mud clast at the middle with a mud drape	Mean grain size (phi)	Mud content (%)	Mean grain-size (phi)	Mud content (%)	Mean grain-size (phi)	Mud content (%)	May 2011
	ON3	38.230361	140.980000	1220	10	Repetition of m. sand and muddy sand layers showing upward fining nearly at the top with a thin mud drape	Mean grain size (phi)	Mud content (%)	Mean grain-size (phi)	Mud content (%)	Mean grain-size (phi)	Mud content (%)	May 2011
	ON4	38.231111	140.978611	1369	10	Repetition of f.-m. sand and muddy sand layers with a thin mud drape	Mean grain size (phi)	Mud content (%)	Mean grain-size (phi)	Mud content (%)	Mean grain-size (phi)	Mud content (%)	May 2011
	ON5	38.231722	140.977444	1496	7	Repetition of f.-m. sand and muddy sand layers with a thin mud drape	Mean grain size (phi)	Mud content (%)	Mean grain-size (phi)	Mud content (%)	Mean grain-size (phi)	Mud content (%)	May 2011

Table 2 (continued)

Area	Location	GPS coordinates		Distance (m)	Thickness (cm)	Description	Tsunami deposit		Underlying soil		Overlying mud drape		Survey Date
		Latitude	Longitude				Mean grain size (phi)	Mud content (%)	Mean grain-size (phi)	Mud content (%)	Mean grain-size (phi)	Mud content (%)	
	ON17	38.245222	140.955056	4030	≈0	Inland limit of the mud drape extent							Apr. 2011
Arahama	AR1	38.215278	140.982083	262	17	*	1.38	2.66	1.48				May 2011
	AR2	38.218194	140.978389	687	4	C. sand including gravels with thin fine sand layer at the top							May 2011
	AR3	38.218194	140.978389	697	9	*	0.74	4.43	1.34				May 2011
	AR4	38.218444	140.978333	722	5	C. sand graded upward into f.-m. sand with a thin mud drape							May 2011
	AR5	38.218444	140.978333	731	9	Repetition of graded layers (c. sand into m. sand) including rip-up clast							May 2011
	AR6	38.218444	140.978333	740	5	C. sand graded upward into m.-c. sand							May 2011
	AR7	38.219472	140.974806	1052	5	C. sand graded upward into m.-c. sand including shell fragments at the bottom with a thin mud drape							May 2011
	AR8	38.220000	140.974333	1118	6	*	1.45	3.11	1.37				May 2011
	AR9	38.222583	140.969083	1661	13	*	1.85	40.97	1.53				Apr. 2011
	AR10	38.222639	140.967556	1784	11	*	1.94	31.77	1.37				Apr. 2011
	AR11	38.224361	140.960944	2366	6.5	*	2.50	62.67	1.68				Apr. 2011

Table 2 (continued)

Area	Location	GPS coordinates		Distance (m)	Thickness (cm)	Description	Tsunami deposit	Underlying soil		Overlying mud drape		Survey Date
		Latitude	Longitude					Mean grain size (phi)	Mud content (%)	Mean grain-size (phi)	Mud content (%)	
	AR12	38.225139	140.958528	2615	6.5	Mud drape						Apr. 2011
	AR13	38.226167	140.954417	2985	4	*	2.06	56.04	1.62	43.23		Apr. 2011
	AR14	38.226361	140.953694	3039	2	F-m. sand with a mud drape						Apr. 2011
	AR15	38.226389	140.953389	3080	1	Mud drape						Apr. 2011
	AR16	38.226361	140.950833	3267	1	Mud drape including f.-m. sand grains						Apr. 2011
	AR17	38.226472	140.950861	3279	0.5	Mud drape including f.-m. sand patches						Apr. 2011
	AR18	38.226722	140.949444	3388	0.2	Thin mud drape						Apr. 2011
	AR19	38.227056	140.948500	3487	0.2	Thin mud drape						Apr. 2011
	AR20	38.227472	140.947028	3617	0.1	Thin mud drape						Apr. 2011
	AR21	38.227750	140.945722	3744	0	No deposit						Apr. 2011
Natori	NT1	38.147250	140.930083	1561	6	C. sand graded upward into f. sand showing laminations with a thin mud drape						May 2011
	NT2	38.147250	140.930083	1579	5	C. sand between thin m. sand layers showing laminations with a thin mud drape						May 2011

Table 2 (continued)

Area	Location	GPS coordinates		Distance (m)	Thickness (cm)	Description	Tsunami deposit		Underlying soil		Overlying mud drape		Survey Date
		Latitude	Longitude				Mean grain size (phi)	Mud content (%)	Mean grain-size (phi)	Mud content (%)	Mean grain-size (phi)	Mud content (%)	
	NT8	38.148611	140.926917	1884	9	Lower c. sand graded upward into muddy f. sand including mud clast, and upper f. sand with a mud drape including plant fragments							May 2011
	NT9	38.148611	140.926917	1895	14	F-m. sand inversely graded upward into well-laminated m. sand, then graded into f-m. sand with a mud drape							May 2011
	NT10	38.143417	140.922528	2052	9	*	1.19	1.29	1.29	4.27			May 2011
	NT11	38.148111	140.912250	3113	2	Mud drape							Apr. 2011
	NT12	38.144139	140.909333	3210	2.3	M. sand with a thin mud drape							Apr. 2011
	NT13	38.148444	140.911056	3231	2	Mud drape							Apr. 2011
	NT14	38.144444	140.908222	3315	3	Mud drape							Apr. 2011
	NT15	38.144639	140.907583	3386	5	Mud drape							Apr. 2011
	NT16	38.146639	140.900778	4036	4	Mud drape							Apr. 2011
Watari	WT1	38.017056	140.915806	164	33	*	1.21	0.60	1.01	14.90			May 2011
	WT2	38.017167	140.914667	269	19	*	1.49	0.38					May 2011

Table 2 (continued)

Area	Location	GPS coordinates		Distance (m)	Thickness (cm)	Description	Tsunami deposit	Underlying soil		Overlying mud drape		Survey Date
		Latitude	Longitude					Mean grain size (phi)	Mud content (%)	Mean grain-size (phi)	Mud content (%)	
	WT15	38.019500	140.890417	2442	7	*	2.75	69.06	0.69	29.16		Jan. 2012
	WT16	38.019528	140.890250	2464	6	Muddy m. sand with a mud drape						May 2011
	WT17	38.018750	140.888139	2620	4	F-m. sand with a mud drape						Apr. 2011
Yamamoto	YM1	37.979722	140.913028	147	46	Repetition of graded layers; m.-c. sand graded upward into m. sand including shell fragments, then it inversely graded into c. sand including gravels. It graded into m. sand including many gravels and laminated f. sand which inversely graded into c. sand, and finally graded into m. sand at the top						Apr. 2011

Table 2 (continued)

Area	Location	GPS coordinates		Distance (m)	Thickness (cm)	Description	Tsunami deposit		Underlying soil		Overlying mud drape		Survey Date
		Latitude	Longitude				Mean grain size (phi)	Mud content (%)	Mean grain-size (phi)	Mud content (%)	Mean grain-size (phi)	Mud content (%)	
	YM19	37.979806	140.881528	2938	2	*	2.55	96.63	1.51	46.07		Apr. 2011	
	YM20	37.979722	140.880361	3040	3	Patchy m.-c. sand at the bottom with a mud drape						May 2011	
	YM21	37.979556	140.879472	3117	2	Patchy f. sand at the bottom with a mud drape including a thin vf.-f. sand layer						May 2011	
	YM22	37.979639	140.878778	3173	1.5	Mud drape						May 2011	
	YM23	37.979306	140.878444	3210	1	Mud drape						May 2011	
	YM24	37.979528	140.877833	3267	0.7	Thin mud drape						May 2011	
	YM25	37.979944	140.877083	3331	0.5	Thin mud drape						May 2011	
	YM26	37.979250	140.876583	3364	7	M. sand with a mud drape						Apr. 2011	
	YM27	37.979194	140.876111	3417	0.5	Thin mud drape						Apr. 2011	
Sujjin-numa	SJ1	37.901361	140.925028	211	27	*	-0.47	1.20				Apr. 2011	
	SJ2	37.901722	140.921056	546	14	*	1.87	3.87	1.76	16.33		Apr. 2011	
	SJ3	37.901556	140.920278	611	13	*	2.42	25.40	1.54	15.79		Apr. 2011	
	SJ4	37.901194	140.918833	739	15	*	0.26	2.16				Apr. 2011	
	SJ5	37.902111	140.918472	757	11	*	2.06	26.95	1.89	34.97		Apr. 2011	
	SJ6	37.901056	140.916194	972	20	Repetition of m.-c. sand graded upward into f.-m. sand with a mud drape						Apr. 2011	
	SJ7	37.900972	140.916028	999	6	*	1.98	14.55	1.54	22.03		Apr. 2011	

Table 2 (continued)

Area	Location	GPS coordinates		Distance (m)	Thickness (cm)	Description	Tsunami deposit		Underlying soil		Overlying mud drape		Survey Date
		Latitude	Longitude				Mean grain size (phi)	Mud content (%)	Mean grain-size (phi)	Mud content (%)	Mean grain-size (phi)	Mud content (%)	
	SJ8	37.899000	140.913583	1262	7	M.-c. sand graded upward into m. sandy mud, with rippled m. sand at the top							Apr. 2011
Shinchi	SJ9	37.897722	140.911083	1515	10	*	1.72	13.71	1.68				Apr. 2011
	SN1	37.883673	140.929535	304	22	*	1.57	3.36	0.86				Jan. 2012
	SN2	37.883595	140.929205	340	19	*	1.69	2.86	1.14				Jan. 2012
	SN3	37.883384	140.928071	443	13	*	1.51	2.85	1.29				Jan. 2012
	SN4	37.883308	140.927401	497	10	*	1.74	5.33	1.27				Jan. 2012
	SN5	37.883265	140.925027	712	5	*	1.99	15.60	1.26				Jan. 2012
	SN6	37.883229	140.923873	810	11	*	1.72	23.74	1.90				Jan. 2012
	SN7	37.882565	140.919536	1203	6	*	1.72	4.11	1.54				Jan. 2012
Odaka	SN8	37.883349	140.915971	1503	6	*	1.67	15.92	1.75				Jan. 2012
	OD1	37.550747	141.019985	809	8	*	1.24	15.15	2.20		30.82	1.41	Nov. 2015
	OD2	37.550484	141.017983	983	12	*	1.04	4.19	2.44		43.72	2.11	Nov. 2015
	OD3	37.550136	141.016356	1133	9	*	1.23	16.94	1.66		65.48	1.81	Nov. 2015
	OD4	37.549779	141.014585	1300	11	*	1.46	6.95	1.73		58.51	2.39	Nov. 2015
	OD5	37.549976	141.012122	1507	9	*	2.17	14.15	2.45		80.69	2.94	Nov. 2015
	OD6	37.550007	141.010755	1620	8	*	2.12	12.63	2.23		72.38	2.72	Nov. 2015
	OD7	37.549174	141.010189	1699	8	*	1.93	11.33	2.33		86.98	2.72	Nov. 2015
	OD8	37.546408	141.004417	2271	0	*			2.41		41.63		Nov. 2015

Descriptions of tsunami deposits are provided for 74 locations where no samples were taken. Asterisks in the "Description" column indicate the 49 sampling locations for which the location-averaged mean grain-size and mud contents of the tsunami deposits and underlying soil (and of the overlying mud drape in the Odaka area) are listed in the neighboring columns on the right. Columnar sections and vertical changes in the grain-size properties of the deposits at these locations are illustrated in Figs. 7, 8, 9, 10, 11 and 12. Detailed descriptions of the locations are provided in Additional file 1



Fig. 2 Aerial views of the eight study areas showing the study locations. The position of each area is shown in Fig. 1B. **A** Onuma area (ON1–17). **B** Arahama area (AR1–21). **C** Natori area (NT1–16). **D** Watari area (WT1–17). **E** Yamamoto area (YM1–27). **F** Suijin-numa area (SJ1–9). **G** Shinchi area (SN1–8). **H** Odaka area (OD1–8). Aerial photographs are from the Geospatial Information Authority of Japan and were taken between December 2012 and September 2013

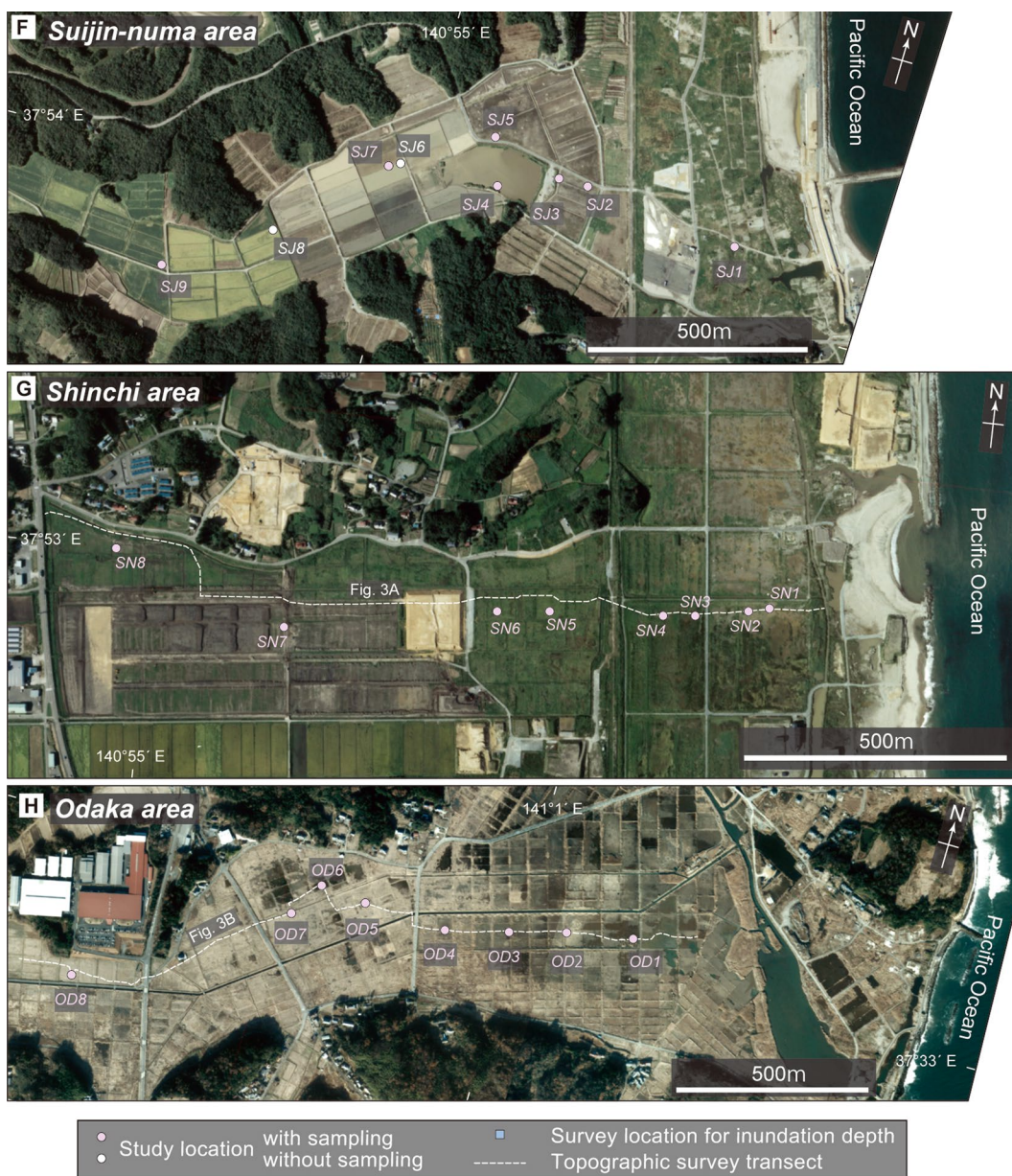


Fig. 2 continued

Table 3 Measured inundation depths and distances from the neighboring coastline

Area	Location	Distance (m)	Inundation depth (cm)
Onuma	ID1	2801	155
	ID2	1733	205
Arahama	ID3	1791	270
	ID4	3062	176
	ID5	3103	126
Natori	ID6	4660	65
Yamamoto	ID7	770	260

capture grain sizes from silt to pebbles. Prior to the grain-size analysis, all samples were subsampled vertically at 1-cm intervals, and the subsamples were sieved in water to remove the mud component. The mud content of each subsample was calculated from the resulting weight reduction. Large pieces of organic matter such as roots and leaves in the subsamples were removed by hand prior to analysis. The measurement range of grain-size analysis was set from -5.25 to $+6.25$ phi at intervals of 0.25 phi. Finally, grain-size distribution properties such as mean grain size and sorting were calculated from the measurements of each subsample using the logarithmic graphical

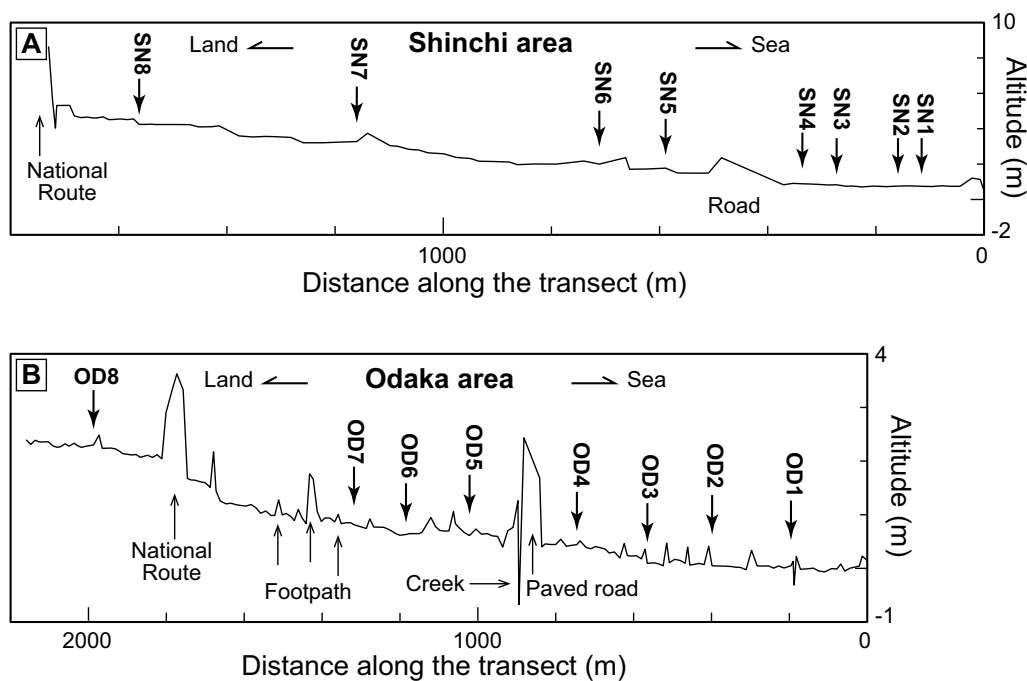


Fig. 3 Topographic profiles along the transects in the **A** Shinchi and **B** Odaka areas; survey transects are indicated in Fig. 2G and H, respectively. Arrows indicate study locations for tsunami deposits. Several tiny peaks indicate footpaths between rice fields

method of Folk and Ward (1957). The average values of these grain-size properties and the mud contents at each location were re-calculated based on the results of the subsamples.

4 Results

4.1 General characteristics of tsunami deposits in the study area

The tsunami deposits were widely distributed over the lowlands in the study areas, and extended up to 4 km inland from the coastline. The tsunami deposits were composed mainly of sand, with occasional gravels, mud clasts, shells, and plant fragments, and sometimes were overlain by a mud drape. The tsunami deposits were easily recognized because they generally overlie the muddy soil of paddy fields or pavement. In addition, the tsunami deposits generally showed an upward-fining trend and parallel lamination, with occasional upward-coarsening or repeated upward-fining trends (Figs. 4, 5, 6, 7, 8 and 9).

The average mud contents of the tsunami deposits and the pre-tsunami deposits (underlying soils) over all locations were 10.6% and 32.9%, respectively. The location-averaged mud contents of the tsunami deposits had a range of 0.4–96.6%. In general, the mud content increased landward, although this pattern varied within study areas (Fig. 10A). In contrast, the location-averaged mud contents of the underlying soils had a range of 2.7–70.3%, and showed no discernible relationship with

distance from the coastline (Fig. 10B). The average mud content of the muddy post-tsunami deposits that were found only in the Odaka area was 71.1%. The location-averaged values of these deposits were 30.8%–87.0% and appeared to show a positive correlation with distance from the coastline (Fig. 10B).

The maximum observed thickness of the tsunami deposits was 65 cm, and the average thickness was 8.6 cm. The thickness decreased exponentially landward; however, the thickness varied widely within each study area (Fig. 11).

The mean grain size of the tsunami deposits averaged over all locations was 1.6 phi, and the range of location-averaged values was -0.5 to $+2.7$ phi. The tsunami deposits showed a faint landward-fining trend, but this varied widely within the study areas (Fig. 12A). The mean grain size of the underlying soil was 1.7 phi, which was not significantly different from that of the tsunami deposits. The range of location-averaged soil grain sizes was 0.7–2.4 phi, and soil grain size appeared to show no relationship with distance from the coastline (Fig. 12B). The mean grain size of the post-tsunami deposits in the Odaka area was on average 2.5 phi, and the location-averaged values were 1.4–2.9 phi, with a landward-fining trend (Fig. 12B). Additionally, the tsunami deposits usually consisted of moderately well-sorted to moderately sorted sand (Figs. 4, 5, 6, 7, 8 and 9; see Additional file 1:

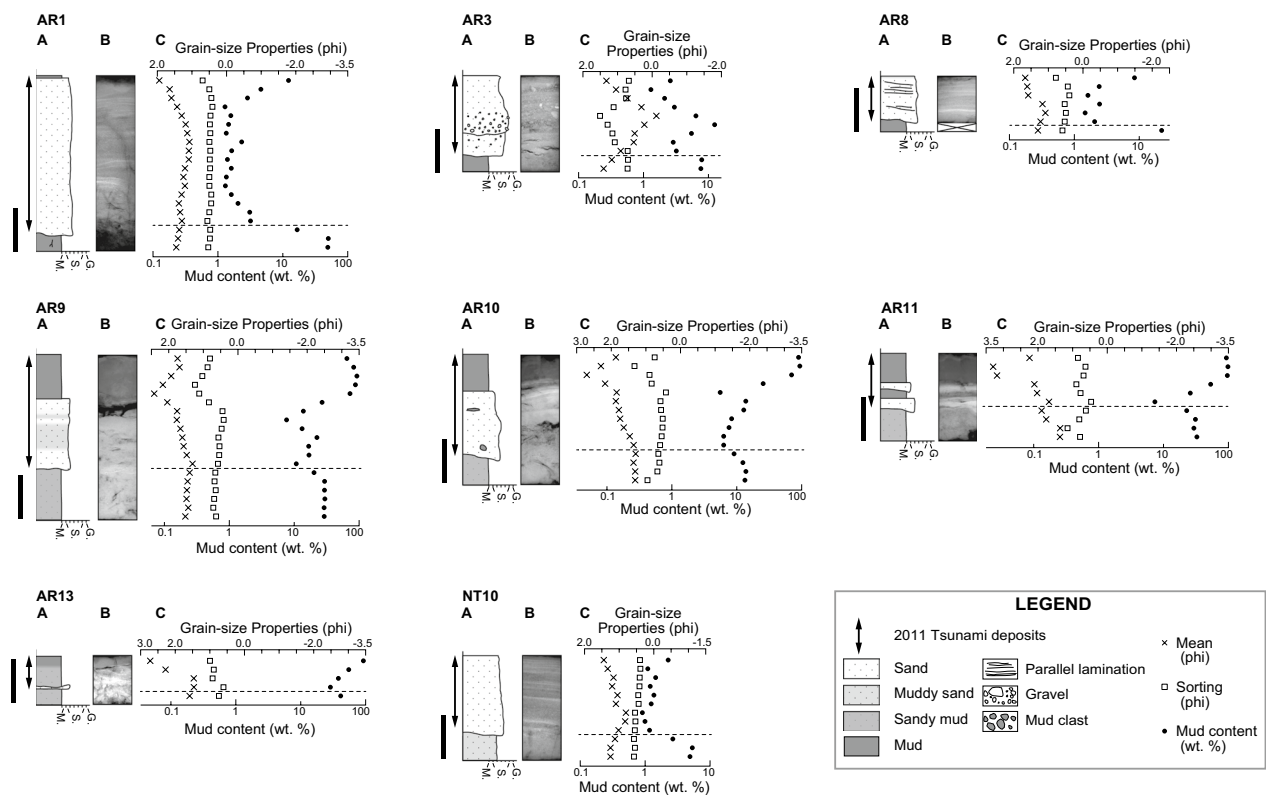


Fig. 4 Schematic diagrams of **A** stratigraphic columns, **B** soft X-ray images, and **C** grain-size analyses at study locations within the Arahama and Natori areas. Scale bars represent 5 cm. Tsunami deposits are indicated by double-headed arrows beside the columns. Horizontal dashed lines in **C** indicate the basal boundary of the tsunami deposits. Mud contents (black circles) are plotted against the bottom logarithmic axis; mean grain sizes (crosses) and sorting values (white squares) are plotted against the top axis

Text S1 and Additional file 2: Data S1 for details), except for muddy layers such as mud drapes.

Normal and inverse grading were common within the tsunami deposits; for example, at location AR1, the tsunami deposits showed inverse and normal grading in the lower and upper parts, respectively, with a gradual upward change in mean grain size from approximately 1.4 phi through 1.1 phi to 2.0 phi (Fig. 4). These grading structures sometimes overlay each other and were associated with mud drapes within the deposits, indicating that the tsunami deposit contained multiple units.

Parallel lamination was also common within the sandy tsunami deposits. The tsunami deposits in this study usually had an erosional contact with the underlying soil, and the lower parts of the tsunami deposits often contained mud clasts and gravel. Below, we describe the sedimentological characteristics of the tsunami deposits in each study area. Detailed descriptions including grain-size data of the tsunami deposits at each location are provided in Table 2, Additional file 1: Text S1 and Additional file 2: Data S1.

4.2 Description of the tsunami deposits in each study area

4.2.1 Onuma Area

The furthest landward inundation limit (5.3 km) and the greatest maximum inundation height (19.7 m) of the study areas occurred in the Onuma and Arahama areas (Table 1). The inundation depth was 155 cm at location ID1 (Fig. 2A, Table 3). Field observations at 17 locations in the Onuma area demonstrated that the tsunami deposits extended about 4 km inland from the coastline and showed an obvious landward-thinning trend: the deposit thickness changed from 14 cm at ON2 (1042 m inland from the coastline) to almost 0 cm at ON17 (4030 m from the coastline) (Fig. 11, Table 2). Visual inspection revealed that the tsunami deposits were generally composed of fine to medium sand, and a mud drape was common at the top of the tsunami deposits. At locations more than 3 km inland from the coastline, the tsunami deposits were predominantly composed of mud.

4.2.2 Arahama area

In the Arahama area, the tsunami reached its furthest inundation limit and highest inundation height, as

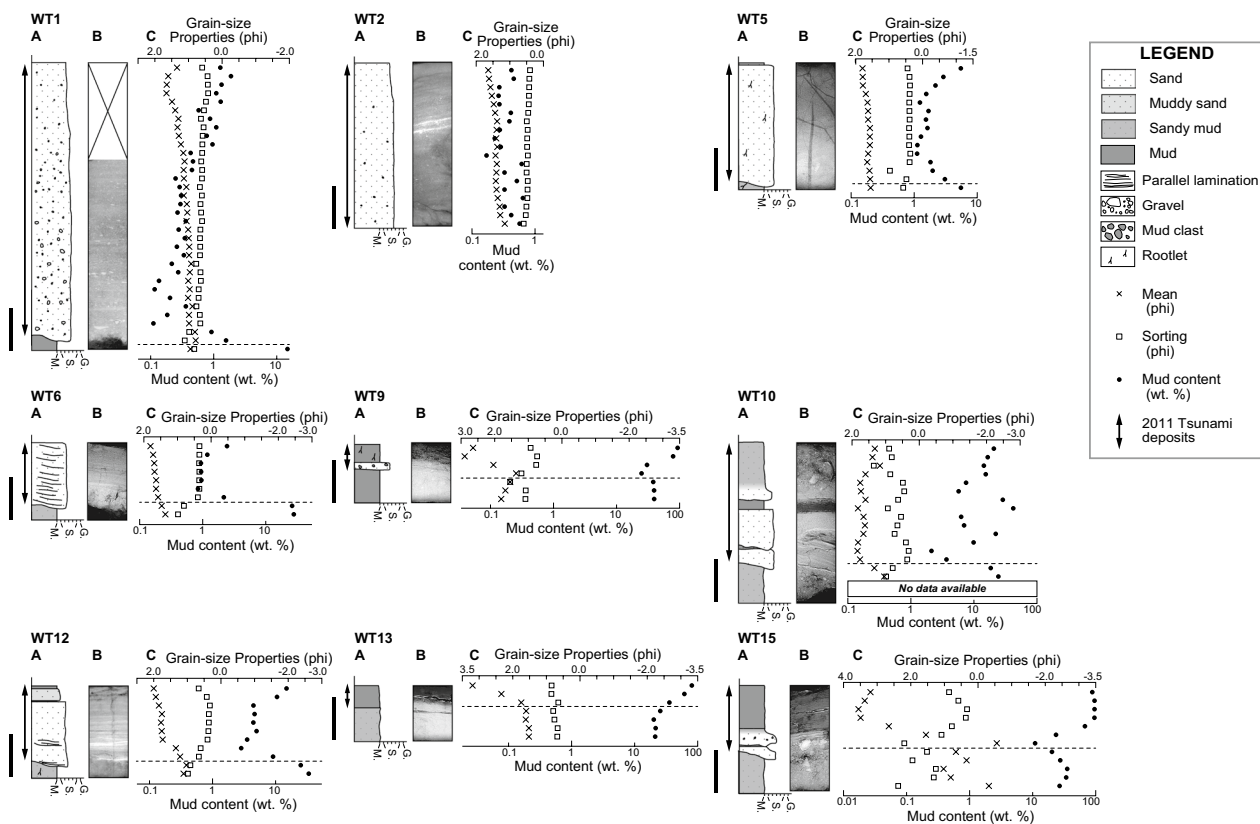


Fig. 5 Schematic diagrams of **A** stratigraphic columns, **B** soft X-ray images, and **C** grain-size analyses at study locations within the Watari area. Scale bars represent 5 cm. Tsunami deposits are indicated by double-headed arrows beside the columns. Horizontal dashed lines in **C** indicate the basal boundary of the tsunami deposits. Mud contents (black circles) are plotted against the bottom logarithmic axis; mean grain sizes (crosses) and sorting values (white squares) are plotted against the top axis

described above. The inundation depths were 205, 270, 176, and 126 cm at locations ID2, ID3, ID4, and ID5, respectively (Fig. 2B and Table 3). Field observations at the 21 sampling locations revealed that the tsunami deposits extended about 3.6 km inland and showed a landward-thinning trend with a wide variation of thicknesses, from 17 cm at AR1 (262 m), to almost 0.1 cm at AR20 (3617 m), and finally disappearing at AR21 (3744 m) (Fig. 11, Table 2). Visual inspection revealed that the tsunami deposits were generally composed of fine to medium sand, and a mud drape was common at the top of the unit (Fig. 4, Table 2). At locations farther than 3 km inland from the coastline, the tsunami deposits were mostly composed of mud drape. Laboratory analysis of samples from seven locations in this area demonstrated that the tsunami deposits had a mean grain size of 1.6 phi with a mud content of 24.0%, whereas the underlying soil had a mean grain size of 1.5 phi and a mud content of 25.4%. The thick mud drape (maximum thickness 5 cm) at the top of the tsunami deposits greatly contributed to the high mud content relative to the soil. The tsunami deposits showed an obvious trend of landward-increasing

mud content and a slight landward-fining trend, whereas the soil showed almost no correlation of those properties with distance from the coastline. An upward-fining trend was also common in the tsunami deposits, but parallel lamination was rare.

4.2.3 Natori area

In the Natori area adjacent to Sendai Airport, field observations at 16 locations demonstrated that the tsunami deposits extended more than 4 km inland, with a wide range of thicknesses from 1 cm at NT6 (1782 m) to 18 cm at NT5 (1730 m) (Fig. 2C, Table 2); thus, in this area, there was almost no trend in thickness with distance from the coastline. Visual inspection revealed that the tsunami deposits were generally composed of medium to coarse sand, occasionally including gravel, and a thin mud drape was commonly present at the top of the tsunami deposits (Table 2). Parallel lamination and upward fining were common in the tsunami deposits, and upward coarsening was rarely observed in this area. At locations more than 3 km from the coastline, the tsunami deposits were predominantly composed of mud. Laboratory

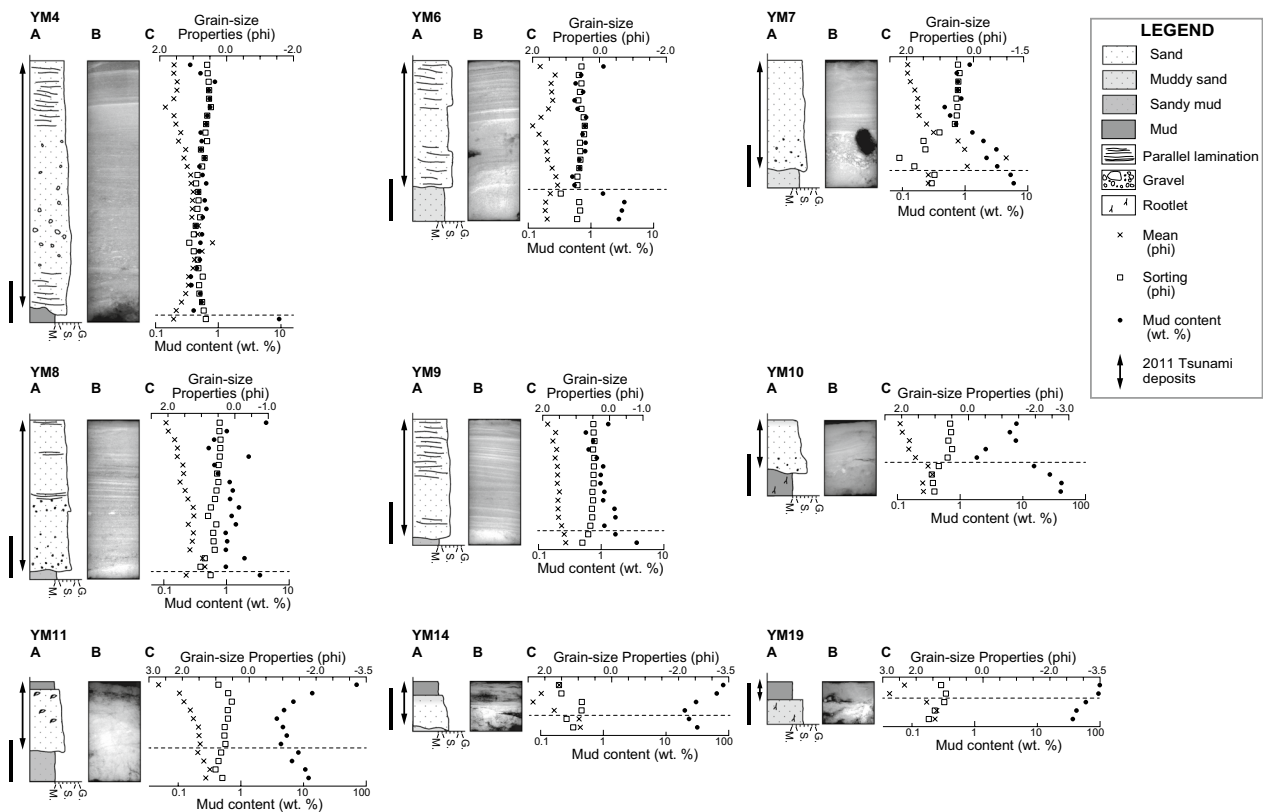


Fig. 6 Schematic diagrams of **A** stratigraphic columns, **B** soft X-ray images, and **C** grain-size analyses at study locations within the Yamamoto area. Scale bars represent 5 cm. Tsunami deposits are indicated by double-headed arrows beside the columns. Horizontal dashed lines in **C** indicate the basal boundary of the tsunami deposits. Mud contents (black circles) are plotted against the bottom logarithmic axis; mean grain sizes (crosses) and sorting values (white squares) are plotted against the top axis

analysis of a sample from location NT10 showed that the tsunami deposits had a mean grain size of 1.2 phi and a mud content of 1.3%, whereas the mean grain size of the underlying soil was 1.3 phi and the mud content was 4.3% (Fig. 4, Table 2).

4.2.4 Watari area

In the Watari area, field observations were carried out at 17 locations. The tsunami deposits were found more than 2.6 km inland and showed a landward-thinning trend, from 33 cm at WT1 (164 m from the coastline) to 3 cm at WT14 (1754 m from the coastline) (Fig. 11, Table 2). Visual inspection revealed that the tsunami deposits were generally composed of fine to medium sand, and a mud drape was occasionally observed at the top of the tsunami unit (Fig. 5, Table 2). The tsunami deposits were predominantly composed of mud at locations more than 1.7 km from the coastline. On the basis of samples from nine locations in this area, the tsunami deposits had a mean grain size of 1.6 phi and a mud content of 11.1%, whereas the grain size of the underlying soil was 1.3 phi and the mud content was 26.5%. The tsunami deposits showed an

increase in mud content and a slight fining trend landward, but the soil showed a faint increase in mud content and almost no trend in mean grain size landward. An upward-fining trend was common in the tsunami deposits, and parallel lamination was occasionally observed.

4.2.5 Yamamoto area

In the Yamamoto area, our field observations at 27 locations demonstrated that the tsunami deposits extended more than 3.4 km inland and showed a clear exponential thinning trend landward, from 65 cm thickness at YM2 (154 m from the coast) to 0.5 cm at YM27 (3417 m from the coast) (Fig. 11, Table 2). Visual inspection revealed that the tsunami deposits were generally composed of fine to medium sand, and, particularly at landward locations, included a mud drape at the top of the unit (Fig. 6, Table 2). At locations more than 2.7 km from the coastline, the tsunami deposits were predominantly composed of mud. Samples from nine locations in this area were analyzed: the tsunami deposits had a mean grain size of 1.5 phi and a mud content of 5.7%, whereas the mean grain size of the underlying soil was 1.4 phi and the mud

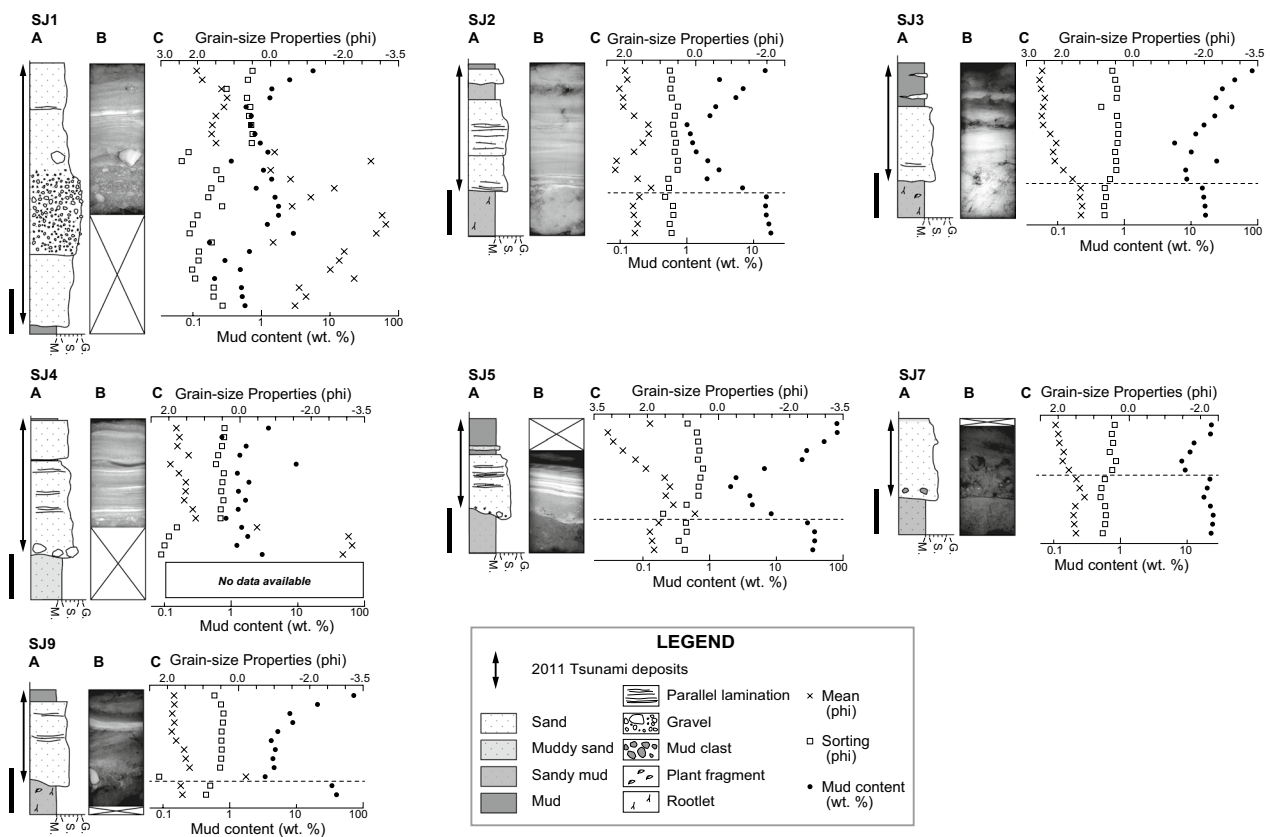


Fig. 7 Schematic diagrams of **A** stratigraphic columns, **B** soft X-ray images, and **C** grain-size analyses at study locations within the Suijin-numa area. Scale bars represent 5 cm. Tsunami deposits are indicated by double-headed arrows beside the columns. Horizontal dashed lines in **C** indicate the basal boundary of the tsunami deposits. Mud contents (black circles) are plotted against the bottom logarithmic axis; mean grain sizes (crosses) and sorting values (white squares) are plotted against the top axis

content was 17.2%. The tsunami deposits showed a clear increase in mud content and became finer landward; the soil showed a clear increase in mud content but an almost constant mean grain size landward. Upward-fining and parallel lamination was common in the tsunami deposits, and upward coarsening was occasionally visible.

4.2.6 Suijin-numa area

In the Suijin-numa area, we carried out field observations at nine locations and identified that the tsunami deposits extended more than 1.5 km inland and showed a faint thinning trend landward, from 27 cm thickness at SJ1 (211 m from the coast) to 6 cm at SJ7 (999 m from the coast) (Fig. 11, Table 2). Visual inspection revealed that the tsunami deposits were generally composed of fine to coarse sand, with gravelly sediments occurring at SJ1 (Fig. 7, Table 2). A mud cap was commonly present at the top of the tsunami deposits (Fig. 7, Table 2). Based on the laboratory analysis of samples from seven locations in this area, the tsunami deposits had a mean grain size of 1.3 phi and a mud content of 10.1%, whereas

the underlying soil had a mean grain size of 1.7 phi and a mud content of 23.3%. The tsunami deposits showed a faint increase in mud content and a faint fining trend landward, albeit with wide variation, but the soil showed a clear increase in mud content and an almost constant mean grain size landward. Upward fining and parallel lamination were common in the tsunami deposits, and upward coarsening was occasionally present.

4.2.7 Shinchi area

In the Shinchi area, a topographic survey demonstrated that the lowland in the narrow valley had a relatively high average gradient of 2‰ within the area of the tsunami deposit (Fig. 3A). Field observations at eight locations demonstrated that the tsunami deposits extended more than 1.5 km inland and gradually thinned landward, from 22 cm at SN1 (304 m from the coast) to 5 cm at SN5 (712 m from the coast) (Fig. 11, Table 2). Visual inspection revealed that the tsunami deposits were mainly composed of medium sand, and a mud cap was common at the top of the unit (Fig. 8). Based on the laboratory

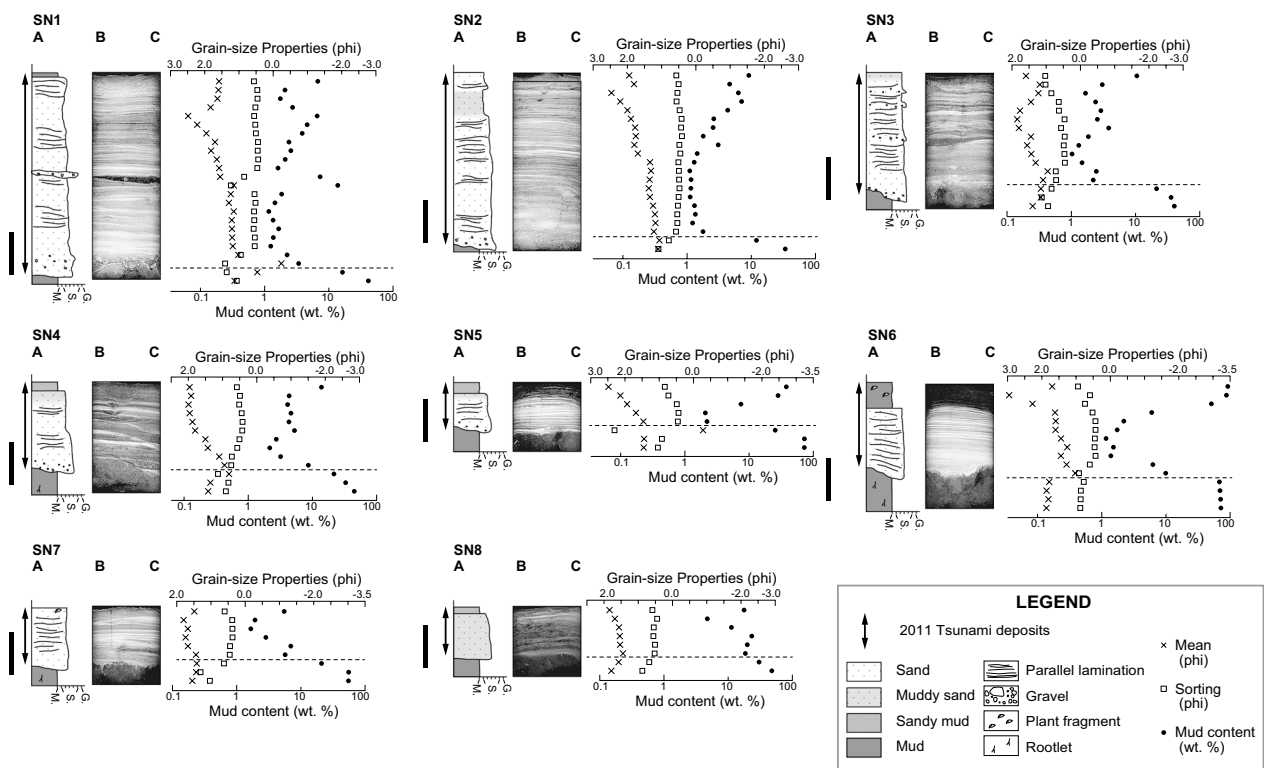


Fig. 8 Schematic diagrams of **A** stratigraphic columns, **B** soft X-ray images, and **C** grain-size analyses at study locations within the Shinchi area. Scale bars represent 5 cm. Tsunami deposits are indicated by double-headed arrows beside the columns. Horizontal dashed lines in **C** indicate the basal boundary of the tsunami deposits. Mud contents (black circles) are plotted against the bottom logarithmic axis; mean grain sizes (crosses) and sorting values (white squares) are plotted against the top axis

analysis of samples from all locations in this area, the mean grain size of the tsunami deposits was 1.7 phi and the mud content was 7.4%, whereas the mean grain size of the underlying soil was 1.4 phi and the mud content was 43.7%. The tsunami deposits showed a faint increase in mud content and almost no trend in mean grain size landward, whereas the mud content and grain size of the soil increased and slightly fined landward, respectively. An upward-fining trend and parallel lamination were very common in the tsunami deposits, and upward coarsening was occasionally observed. These upward coarsening–fining trends were repeated, especially at locality SN3.

4.2.8 Odaka area

In the Odaka area, a topographic survey revealed that the lowland in the narrow valley had a relatively high average gradient of 1‰ within the area of the tsunami deposits (Fig. 3B). Field observations at eight locations demonstrated that the tsunami deposits extended to a distance of 1.7 km inland. Visual inspection revealed that the deposits were mainly composed of fine to medium sand and showed a gradual upward change from sand

to muddy sand and/or sandy mud, and finally a thick mud cap at the top, which was characteristic of the tsunami unit in this area (Fig. 9). Distinguishing the tsunami deposits from post-tsunami reworked sediments was difficult in this area, because our survey was conducted 4 years after the tsunami. Here we define the tsunami deposits as layers of sand and muddy sand, and post-tsunami deposits as layers of mud and sandy mud, though some uncertainty about these identifications remains. Abundant rootlets were found penetrating the post-tsunami deposits toward the top of the tsunami deposits. The tsunami deposits showed a faint landward-thinning trend from 12 cm at OD2 (983 m from the coast), to 8 cm at OD7 (1699 m from the coast), and finally disappearing at OD8 (2271 m from the coast) (Fig. 11, Table 2). Samples from all locations in this area were analyzed. The tsunami deposits had a mean grain size of 1.6 phi and a mud content of 11.1%; the corresponding values for the underlying soil were 2.2 phi and 46.9%, respectively. The tsunami deposits contained an almost constant percentage of mud and become slightly finer landward, whereas the soil showed no trend in mud content and almost constant mean grain size. The thick mud cap (mud content

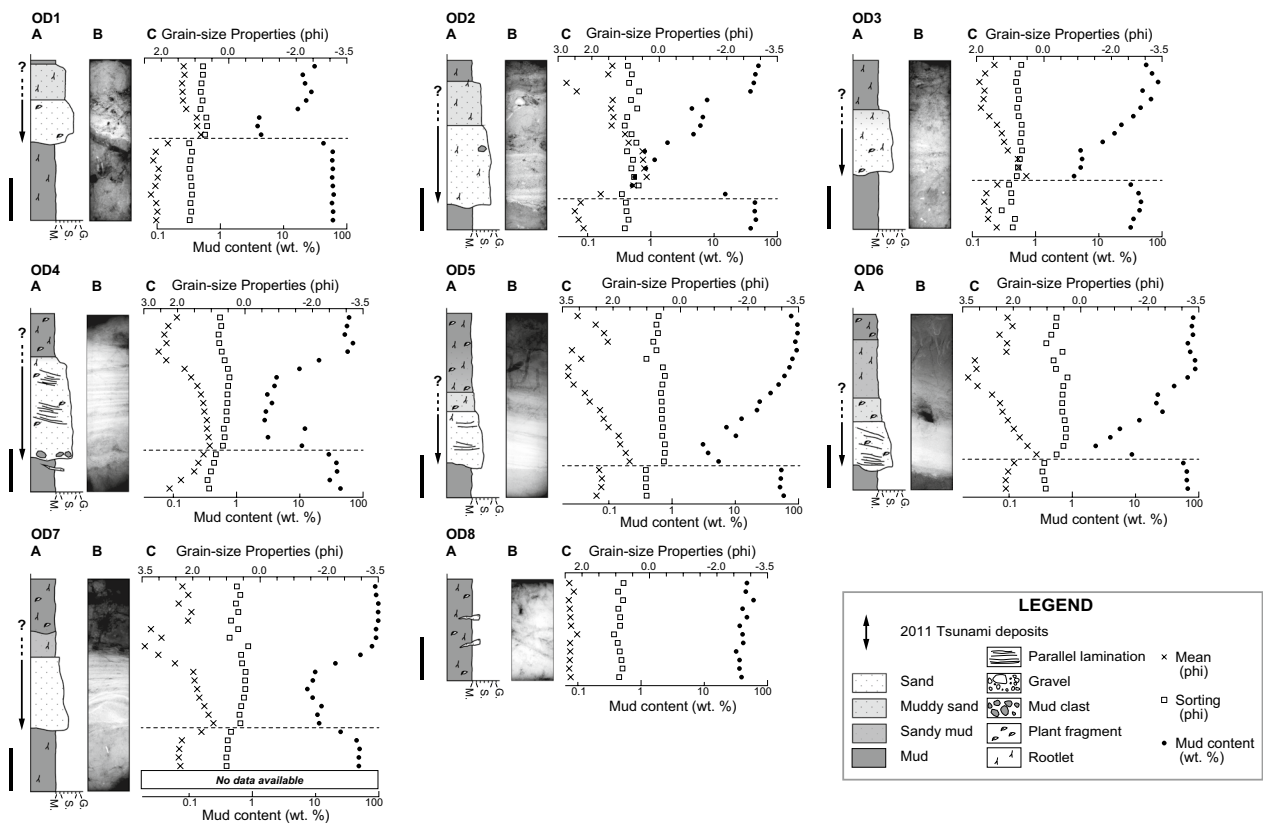


Fig. 9 Schematic diagrams of **A** stratigraphic columns, **B** soft X-ray images, and **C** grain-size analyses at study locations within the Odaka area. Scale bars represent 5 cm. Tsunami deposits are indicated by double-headed arrows beside the columns. Horizontal dashed lines in **C** indicate the basal boundary of the tsunami deposits. Mud contents (black circles) are plotted against the bottom logarithmic axis; mean grain sizes (crosses) and sorting values (white squares) are plotted against the top axis

71.1%) at the top had a mean grain size of 2.5 phi and showed a clear increase in mud content and a gradual fining trend landward. Within the tsunami unit, upward fining and parallel lamination were very common, and mud clasts and plant fragments were occasionally present. Additionally, rootlets penetrating down into the tsunami deposits were well developed in this area.

5 Discussion

5.1 Spatial distribution of tsunami deposits

The wide extent of tsunami inundation and the spatial distribution of tsunami deposits may be attributed to the low-gradient topography of the study areas, where the average gradient is 0.3–3%. In contrast, in areas with steeper gradients, the distribution of tsunami deposits is generally limited; for example, Goto et al. (2017) found gravelly tsunami deposits within approximately 1 km of the coastline with an average gradient of ca. 2% in a narrow valley on the ria-type Sanriku coast. Naruse et al. (2012) reported the presence of tsunami deposits within approximately 1.5 km of the coastline in a bay-head delta on the Sanriku coast, where the average gradient is 1%.

The tsunami inundation limit and the distribution of tsunami deposits are controlled by the gradient and the surrounding environment.

Our observations revealed that the widely distributed tsunami deposits on the Sendai Plain and the northern coast of Fukushima Prefecture generally showed a landward-thinning trend. This trend is a common feature of the 2011 tsunami deposits (e.g., Goto et al. 2011; Abe et al. 2012, 2020; Richmond et al. 2012; Matsumoto et al. 2016) and other tsunami deposits elsewhere (e.g., Gelfenbaum and Jaffe 2003; Hori et al. 2007; Fujino et al. 2010), suggesting a general landward decrease in the flow capacity of tsunamis (Hiscott 1994). Goto et al. (2011) reported that the 2011 tsunami deposits became thin and mud-dominated landward around Sendai Airport, near the Natori area of this study. Abe et al. (2020) and Iijima et al. (2021) also studied the 2011 tsunami deposits in narrow valleys near Suijin-numa and in the Odaka area, respectively. Both studies concluded that the deposits generally thinned landward; however, there were some fluctuations resulting from the micro-geomorphology and artificial structures. These results are concordant with our

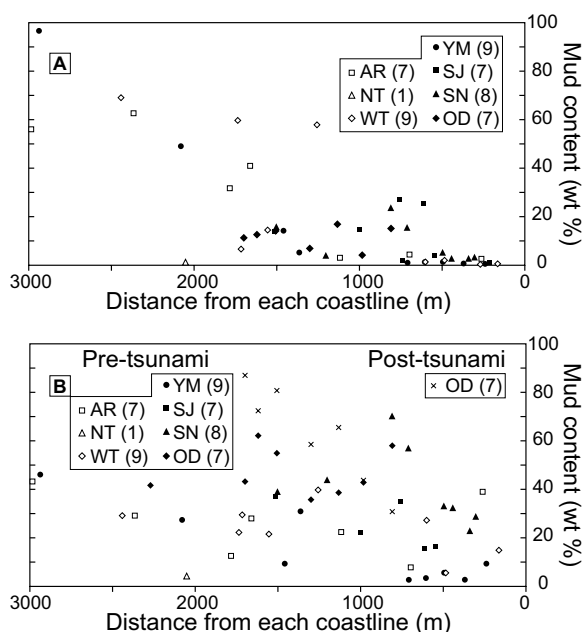


Fig. 10 Average mud contents at each location with distance from the coastline within each study area. **A** Mud contents of the tsunami deposits. **B** Mud contents of the pre- and post-tsunami deposits

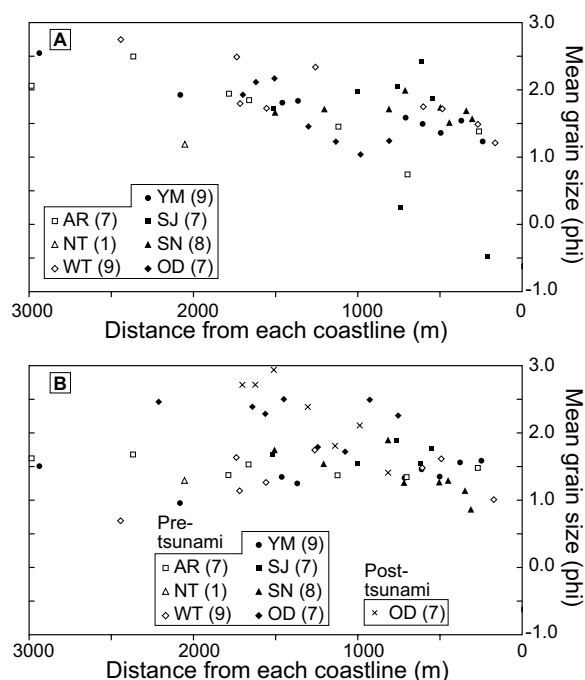


Fig. 12 Mean grain sizes with distance from the coastline within each study area. The mean grain size is the average value for each location. **A** Mean grain sizes of the tsunami deposits. **B** Mean grain sizes of the pre- and post-tsunami deposits

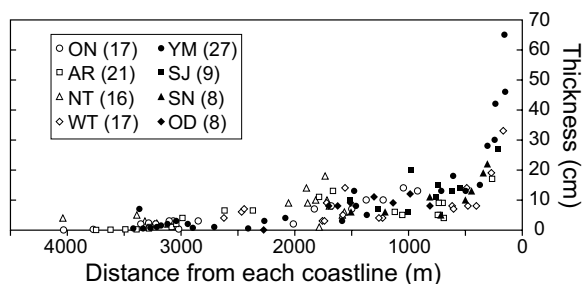


Fig. 11 Thicknesses of tsunami deposits with distance from the coastline within each study area

findings that there is an overall landward-thinning trend, but some non-negligible fluctuations occur in each area.

5.2 Grain-size composition

The mud content of the tsunami deposits as a whole tended to obviously increase with distance from the coastline (Fig. 10A), concomitant with the landward-fining trend (Fig. 12A), whereas the mud content and mean grain size of the underlying soil did not seem to correlate with distance from the coast (Figs. 10B, 12B). These trends in the tsunami deposits have been reported by previous studies in the Sendai Plain (e.g., Goto et al. 2011; Abe et al. 2012, 2020), and can be explained by the continual entrainment of mud from the surface soil

(Nanayama and Shigeno 2006; Matsumoto et al. 2010; Iijima et al. 2021) and the selective sedimentation of coarser grains (Bondevik et al. 1997; Fujino et al. 2010) during landward inundation. However, the mud content in each area did not tend to show a regular increase, especially in the three southern areas. Abe et al. (2020) studied a location very near the Suijin-numa area in this study and showed that the thicknesses of the mud layers of tsunami deposits, such as mud drapes, varied independently of the inundation distance or topographic elevation. They concluded that the thicknesses of the mud layers were affected by sediments from Suijin-numa Pond located in the middle of the valley.

Diversity in the grain-size composition of the tsunami deposits was recognized in this study, although the deposits were composed mainly of well-sorted sandy sediments at most locations. For example, the tsunami deposit at SJ1 was characterized by gravelly sediments, and the tsunami deposits in the Odaka area were characterized by thick mud drapes at their tops (Figs. 7, 9). These variations in tsunami deposits are commonly recognized for the deposits formed by modern and paleo events in the Sendai and Fukushima regions and elsewhere (e.g., Hori et al. 2007), and can result from various factors; for example, bedforms formed under inundation flow and influenced by the return flow might enhance

vertical and horizontal grain-size deviations. In general, tsunamis hit wide areas that contain a range of environments, so it is difficult to specify the factor(s) causing the diversity; however, differences in sediment sources along coastal zones and variations in the depositional processes owing to topographic differences are possible causes (e.g., Szczuciński et al. 2012; Goto et al. 2017; Abe et al. 2020). Such diversity in grain-size composition and in sedimentary structures, as mentioned below, makes it difficult to identify paleo-tsunami deposits. In most cases, it is necessary to combine multiple features as supporting evidence for paleo-tsunami deposits (Goff et al. 2012; Sawai 2012). Thus, consideration of the diversity of sedimentary features of modern tsunami deposits is important when identifying paleo-tsunami deposits.

5.3 Sedimentary structures

The grain-size properties and sedimentary structures of the tsunami deposits in this study reflect the sedimentary processes under the inundation flow at each location. Normal grading was the most common structure in the tsunami deposits in this study and has also commonly been found in other paleo- and modern tsunami deposits (e.g., Dawson and Shi 2000; Hori et al. 2007; Jankaew et al. 2008). Normal grading results from suspension settling or bedload during the waning of the flow (Naruse et al. 2012). In this study, normal grading was frequently associated with parallel lamination. These combined features were observed within about 1.1 km of the coast on the Sendai Plain and 1.6 km of the coast in the three southern areas, implying that these sediments were deposited from bedload under relatively rapid flow, as mentioned below. In contrast, normal grading without parallel lamination was mainly found at locations further inland and might have resulted from suspension settling under relatively slow flow or in stagnant water. Inverse grading was also observed in this study and has been documented in other modern tsunami deposits (e.g., Hori et al. 2007; Paris et al. 2007; Sawai et al. 2009a; Naruse et al. 2010, 2012). Inverse grading results from flow acceleration during the waxing stage (Naruse et al. 2010; Iijima et al. 2021) or a traction carpet under sheet flow (Sohn 1997; Moore et al. 2011), indicating a considerable flow. This suggestion is consistent with the fact that inverse grading was observed in the relatively thick tsunami deposits within approximately 700 m of the coast. Multiple-unit structures usually consist of repeated sets of normal and/or inverse grading, suggesting multiple stages of inundation and/or return flows (Hori et al. 2007; Paris et al. 2007; Naruse et al. 2010, 2012).

Parallel lamination was commonly detected in this study, including by soft X-ray imaging (Figs. 4, 5, 6, 7, 8

and 9, Table 2). In this study, parallel lamination was typically recognized in tsunami deposits that have a thickness of more than 5 cm. The tsunami deposits showing parallel lamination were detected as far as approximately 1.7 km inland. These structures are formed by low-amplitude bedforms under a plane-bed flow regime (Allen 1984; Best and Bridge 1992), suggesting that the inundation flow had a relatively high velocity during the deposition of these sediments. In contrast, cross-lamination/ripple marks were not found in this study, except at location SJ8 (Table 2), and have rarely been reported in other studies (e.g., Naruse et al. 2012; Takashimizu et al. 2012). The scarcity of cross-lamination/ripple marks might imply that there were almost no cases in which the tsunami inundation flow continuously maintained a lower flow regime.

Mud drapes were recognized in the tsunami deposits at 83 locations over the study areas (Figs. 4, 5, 6, 7, 8 and 9, Table 2). These drapes were formed from suspension during the stagnant stage of the inundation flow. Therefore, the presence of mud drapes suggests that multiple flows were produced by the tsunami (Fujiwara and Kamataki 2007). Mud drapes have previously been found in the 2011 tsunami deposits (e.g., Naruse et al. 2012; Abe et al. 2020) and other modern tsunami deposits (e.g., Nanayama and Shigeno 2006; Choowong et al. 2008; Matsumoto et al. 2008; Naruse et al. 2010).

The lower contact of the tsunami deposits in this study was usually a gently undulating sharp erosional surface, often with mud clasts and basal gravels on the surface, suggesting that the strong flow eroded the existing muddy surface to form the tsunami deposits. Some studies have reported that deformation structures such as load casts occur at the contact between tsunami deposits and underlying soft sediments for both ancient (Minoura and Nakata 1994; Sawai et al. 2015) and modern (Matsumoto et al. 2008) tsunamis; however, such structures were rarely found at the lower contact of the tsunami deposits in this study. This absence is probably because most of the tsunami deposits in this study were deposited on rice fields during the fallow period, a relatively hard preexisting surface that resisted deformation.

5.4 Application to paleo-tsunami research

The differences between the tsunami deposits in the Odaka area and those in the other areas might imply the occurrence of post-depositional alteration, because the field observation in the Odaka area was conducted 3–4 years after that in the other areas. In fact, it is necessary to consider environmental differences: the tsunami deposits in the Odaka area uniquely possessed thick mud drapes at their tops that were possible post-tsunami

reworked sediments (Fig. 9). The lower boundary of the tsunami deposits was clearly sharp, as in the other areas; in contrast, the top boundary was vague, possibly because of downward bioturbation by intruding rootlets. Spiske et al. (2020) demonstrated that post-depositional alteration decreased the thickness and mean grain size of the tsunami deposits, and similar processes would have occurred in the Odaka area. Such post-depositional alteration of tsunami deposits could cause problems when identifying paleo-tsunami deposits and using them to reconstruct the magnitude of tsunami events. In this respect, long-term observation of modern tsunami deposits is required for more precise paleo-tsunami research.

Abe et al. (2012) proposed a 1:1 relationship between the maximum inundation distance and the extent of sandy tsunami deposits. They concluded that the relationship was valid up to 2.5 km inland, and the maximum extent of recognizable deposits (≥ 0.5 cm) was limited to within 3 km of the coast. Some differences appear when plotting the data in this study (Fig. 13): the relationship seems to be generally valid up to 3.5 km inland, and the maximum extent of sandy deposits is limited to within 3.4 km of the coast. Moreover, in places where the maximum inundation distance exceeded 5 km and the relationship is totally invalid, a large gap is recognized between the extent of sand and the distribution of mud drapes. Some of these differences might arise from the sparsity of data; however, the fact that a similar tendency

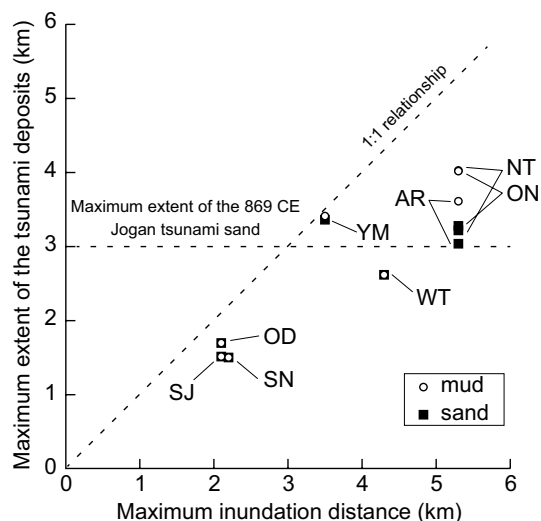


Fig. 13 Scatter plot showing the maximum inundation distance and extent of tsunami deposits within the eight study areas. Mud drapes were found further inshore than sand in the Onuma, Arahama, Natori, and Yamamoto areas. The two dashed lines are after Fig. 9 of Abe et al. (2012), which referred to Sugawara et al. (2010) regarding the maximum extent of the 869 CE Jogan tsunami deposits

was recognized in this study is important for future paleo-tsunami research.

The large amount of data on modern tsunami deposits provided in this study can be used to validate numerical modeling methods, leading to a more precise estimation of the hydraulic conditions of paleo-tsunamis from their deposits. However, some issues still remain, including the precise estimation of maximum inundation distance and post-depositional alteration. Along with the sedimentological data in this study, geochemical (Chagué-Goff 2010) and microfossil (Hemphill-Haley 1996) approaches will help to identify the maximum inundation distance from the deposits, as pointed out by Goto et al. (2011). Finally, it will be possible to evaluate how post-depositional processes have altered deposits by comparing paleo-tsunami deposits and the results of numerical simulations (Spiske et al. 2020). In this regard, the Sendai Plain, where extensive research on the 869 CE Jogan tsunami deposits has been conducted, would be the best place to conduct such a comparative study.

6 Conclusions

We described the 2011 Tohoku-oki tsunami deposits on the Sendai and Fukushima coasts, with quantitative data on their thickness and grain size at 1-cm vertical intervals along transects. The sedimentary characteristics of the 2011 tsunami deposits can be summarized as follows: (1) The tsunami deposits in the study areas extended up to 4 km inland, probably owing to the overall low-gradient topography. (2) The tsunami deposits showed landward-fining and landward-thinning trends with minor fluctuations, and also a trend of landward increase in the mud content. (3) Diversity in the grain-size composition of the tsunami deposits was recognized, resulting from differences in the sediment source and possibly topographic conditions. (4) Normal grading, parallel lamination, and mud drapes were found widely over the study areas, whereas inverse grading and cross-lamination/ripple marks were recognized at only limited locations. (5) The lower contact of the studied tsunami deposits is clearly sharp; however, the top boundary is vague in the Odaka area, possibly owing to the influence of post-depositional alteration. (6) The 1:1 relationship proposed by Abe et al. (2012) is valid only up to 3.5 km inland in this study.

These findings will contribute to a better understanding of modern and paleo-tsunami deposits. Furthermore, the vertically high-resolution dataset representing a range of environments provided in this study will be useful to validate numerical modeling methods, leading to progressive enhancement of the spatial and temporal resolution of estimates of the hydraulic conditions of inundation flows,

and improved evaluation of the degree of post-depositional alteration processes.

Abbreviations

VRS Virtual Reference Station
GNSS Global Navigation Satellite System

Supplementary Information

The online version contains supplementary material available at <https://doi.org/10.1186/s40645-023-00553-3>.

Additional file 1. Detailed descriptions of the tsunami deposits at each location in eight study areas.

Additional file 2. Results of grain-size analysis in this study (volume fraction, %). The gray cells indicate results for the underlying soil. The underlined values indicate results for the supposed post-tsunami sediments.

Acknowledgements

We would like to thank Yukinobu Okamura for assistance in the field survey. Thomas Kosciuch and Jessica Pilarczyk read an early version of the manuscript and gave valuable comments. This manuscript was substantially improved by valuable suggestions and comments from two anonymous reviewers and the associate editor Dr. Masaki Yamada.

Author contributions

YS participated in all fieldwork. YN and MS took part in fieldwork in Onuma, Arahama, Natori, Watari, Yamamoto, and Sujjin-numa; KT participated in fieldwork in Onuma, Arahama, Natori, Watari, Yamamoto, Shinchi, and Odaka; KK and OF took part in fieldwork in Onuma, Arahama, and Natori; and DM and TS participated in fieldwork in Shinchi and Odaka. YS recorded preliminary field descriptions in Sendai and Shinchi. YS and DM carried out soft X-ray imaging in the laboratory. DM described detailed sedimentary features in the laboratory, carried out the grain-size analysis, and prepared the manuscript including tables, figures, and additional files. All authors read and approved the final manuscript.

Funding

This work was partially supported by JSPS KAKENHI Grant Number 15K05334.

Availability of data and materials

Data sharing is not applicable to this article as no datasets were generated or analyzed during the current study. Please contact the corresponding author for data requests.

Declarations

Competing interests

The authors declare that they have no competing interest.

Received: 24 August 2022 Accepted: 12 April 2023

Published online: 04 May 2023

References

- Abe T, Goto K, Sugawara D (2012) Relationship between the maximum extent of tsunami sand and the inundation limit of the 2011 Tohoku-oki tsunami on the Sendai Plain, Japan. *Sediment Geol* 282:142–150
- Abe T, Goto K, Sugawara D (2020) Spatial distribution and sources of tsunami deposits in a narrow valley setting—insight from 2011 Tohoku-oki tsunami deposits in northeastern Japan. *Prog Earth Planet Sci* 7:1–21
- Allen JRL (1984) Parallel lamination developed from upper-stage plane beds: a model based on the larger coherent structures of the turbulent boundary layer. *Sediment Geol* 39:227–242
- Best JL, Bridge JS (1992) The morphology and dynamics of low amplitude bedwaves upon upper stage plane beds and the preservation of planar laminae. *Sedimentology* 39:737–752
- Bondevik S, Svendsen JI, Mangerud J (1997) Tsunami sedimentary facies deposited by the Storegga tsunami in shallow marine basins and coastal lakes, western Norway. *Sedimentology* 44:1115–1131
- Cisternas M, Atwater BF, Torrejón F, Sawai Y, Machuca G, Lagos M, Eipert A, Youlton C, Salgado I, Kamataki T, Shishikura M, Rajendran CP, Malik JK, Rizal Y, Husni M (2005) Predecessors of the giant 1960 Chile earthquake. *Nature* 437:404–407. <https://doi.org/10.1038/nature03943>
- Chagué-Goff C (2010) Chemical signatures of palaeotsunamis: a forgotten proxy? *Mar Geol* 271:67–71
- Chagué-Goff C, Andrew A, Szczucinski W, Goff J, Nishimura Y (2012a) Geochemical signatures up to the maximum inundation of the 2011 Tohoku-oki tsunami – implications for the 869 AD Jogan and other palaeotsunamis. *Sediment Geol* 282:65–77
- Chagué-Goff C, Niedzielski P, Wong HKY, Szczucinski W, Sugawara D, Goff J (2012b) Environmental impact assessment of the 2011 Tohoku-oki tsunami on the Sendai plain. *Sediment Geol* 282:175–187
- Choowong M, Murakoshi N, Hisada K, Charusiri P, Charoentitrat T, Chutakositkanon V, Jankaew K, Kanjanapayont P, Phantuwongraj S (2008) 2004 Indian Ocean tsunami inflow and outflow at Phuket, Thailand. *Mar Geol* 248:179–192. <https://doi.org/10.1016/j.margeo.2007.10.011>
- Dawson A, Shi S (2000) Tsunami deposits. *Pure Appl Geophys* 157:875–897
- Dura T, Horton BP, Cisternas M, Ely LL, Hong I, Nelson AR, Wesson RL, Pilarczyk JE, Parnell AC, Nikitina D (2017) Subduction zone slip variability during the last millennium, south-central Chile. *Quat Sci Rev* 175:112–137. <https://doi.org/10.1016/j.quascirev.2017.08.023>
- Folk RL, Ward WC (1957) Brazos River bar: a study in the significance of grain size parameters. *J Sediment Petrol* 27:3–26
- Fujino S, Naruse H, Matsumoto D, Sakakura N, Suphawajraksakul A, Jarupongsakul T (2010) Detailed measurements of thickness and grain size of a widespread onshore tsunami deposit in Phang-nga Province, southwestern Thailand. *Island Arc* 19:389–398. <https://doi.org/10.1111/j.1440-1738.2010.00730.x>
- Fujiwara O, Kamataki T (2007) Identification of tsunami deposits considering the tsunami waveform: an example of subaqueous tsunami deposits in Holocene shallow bay on southern Boso Peninsula, Central Japan. *Sediment Geol* 200:295–313. <https://doi.org/10.1016/j.sedgeo.2007.01.009>
- Fujino S, Kimura H, Komatsubara J, Matsumoto D, Namegaya Y, Sawai Y, Shishikura M (2018) Stratigraphic evidence of historical and prehistoric tsunamis on the Pacific coast of central Japan: Implications for the variable recurrence of tsunamis in the Nankai Trough. *Quat Sci Rev* 201:147–161. <https://doi.org/10.1016/j.quascirev.2018.09.026>
- Gelfenbaum G, Jaffe B (2003) Erosion and sedimentation from the 17 July, 1998 Papua New Guinea Tsunami. *Pure Appl Geophys* 160:1969–1999. <https://doi.org/10.1007/s00024-003-2416-y>
- Goff J, Chagué-Goff C, Nichol S, Jaffe B, Dominey-Howes D (2012) Progress in palaeotsunami research. *Sediment Geol* 243–244:70–88. <https://doi.org/10.1016/j.sedgeo.2011.11.002>
- Goto K, Chagué-Goff C, Fujino S, Goff J, Jaffe B, Nishimura Y, Richmond B, Sugawara D, Szczucinski W, Tappin DR, Witter RC, Yulianto E (2011) New insights of tsunami hazard from the 2011 Tohoku-oki event. *Mar Geol* 290:46–50
- Goto K, Fujima K, Sugawara D, Fujino S, Imai K, Tsudaka R, Abe T, Haraguchi T (2012) Field measurements and numerical modeling for the run-up heights and inundation distances of the 2011 Tohoku-oki tsunami at Sendai Plain, Japan. *Earth Planets Space* 64:1247–1257
- Goto K, Hashimoto K, Sugawara D, Yanagisawa H, Abe T (2014) Spatial thickness variability of the 2011 Tohoku-oki tsunami deposits along the coastline of Sendai Bay. *Mar Geol* 358:38–48. <https://doi.org/10.1016/j.margeo.2013.12.015>
- Goto T, Satake K, Sugai T, Ishibe T, Harada T, Gusman AR (2017) Effects of topography on particle composition of 2011 tsunami deposits on the ria-type Sanriku coast, Japan. *Quat Int* 456:17–27

- Hemphill-Haley E (1996) Diatoms as an aid in identifying late-Holocene tsunami deposits. *Holocene* 6:439–448
- Higaki H, Goto K, Yanagisawa H, Sugawara D, Ishizawa T (2021) Three thousand year paleo-tsunami history of the southern part of the Japan Trench. *Prog Earth Planet Sci* 8:28. <https://doi.org/10.1186/s40645-021-00415-w>
- Hiscott RN (1994) Loss of capacity, not competence, as the fundamental process governing deposition from turbidity currents. *J Sediment Res* A64:209–214
- Hori K, Kuzumoto R, Hirouchi D, Umitsu M, Janjirawuttikul N, Patanakanog B (2007) Horizontal and vertical variation of 2004 Indian tsunami deposits: an example of two transects along the western coast of Thailand. *Mar Geol* 239:163–172. <https://doi.org/10.1016/j.margeo.2007.01.005>
- Iijima Y, Goto K, Sugawara D, Abe T (2021) Effect of artificial structures on the formation process of the 2011 Tohoku-oki tsunami deposits. *Sediment Geol* 423:105978. <https://doi.org/10.1016/j.sedgeo.2021.105978>
- Ishizawa T, Goto K, Yokoyama Y, Miyairi Y, Sawada C, Nishimura Y, Sugawara D (2017) Sequential radiocarbon measurement of bulk peat for high-precision dating of tsunami deposits. *Quat Geochronol* 41:202–210. <https://doi.org/10.1016/j.quageo.2017.05.003>
- Ishizawa T, Goto K, Yokoyama Y, Miyairi Y (2019) Non-destructive analyses to determine appropriate stratigraphic level for dating of tsunami deposits. *Mar Geol* 412:19–26. <https://doi.org/10.1016/j.margeo.2019.02.009>
- Jaffe BE, Gelfenbaum G (2007) A simple model for calculating tsunami flow speed from tsunami deposits. *Sediment Geol* 200:347–361
- Jaffe BE, Goto K, Sugawara D, Richmond BM, Fujino S, Nishimura Y (2012) Flow speed estimated by inverse modeling of sandy tsunami deposits: results from the 11 March 2011 tsunami on the coastal plain near the Sendai Airport, Honshu, Japan. *Sediment Geol* 282:90–109
- Jankaew K, Atwater BF, Sawai Y, Choowong M, Charoentitirat T, Martin ME, Prendergast A (2008) Medieval forewarning of the 2004 Indian Ocean tsunami in Thailand. *Nature* 455:1228–1231. <https://doi.org/10.1038/nature07373>
- Kelsey HM, Nelson AR, Hemphill-Haley E, Witter RC (2005) Tsunami history of an Oregon coastal lake reveals a 4600 yr record of great earthquakes on the Cascadia subduction zone. *Geol Soc Am Bull* 117:1009–1032
- MacInnes BT, Weiss R, Bourgeois J, Pinegina K (2010) Slip distribution of the 1952 Kamchatka great earthquake based on near-field tsunami deposits and historical records. *Geol Soc Am Bull* 100:1695–1709
- Matsumoto D, Naruse H, Fujino S, Surphawajruksakul A, Jarupongsakul T, Sakakura N, Murayama M (2008) Truncated flame structures within a deposit of the Indian Ocean Tsunami: evidence of syn-sedimentary deformation. *Sedimentology* 55:1559–1570
- Matsumoto D, Sawai Y, Tanigawa K, Fujiwara F, Namegaya Y, Shishikura M, Kagohara K, Kimura H (2016) Tsunami deposit associated with the 2011 Tohoku-oki tsunami in the Hasunuma site of the Kujukuri coastal plain, Japan. *Island Arc* 25:369–385. <https://doi.org/10.1111/iar.12161>
- Matsumoto D, Shimamoto T, Hirose T, Gunatilake J, Wickramasooriya A, DeLile J, Young S, Rathnayake C, Ranasooriya J, Murayama M (2010) Thickness and grain-size distribution of the 2004 Indian Ocean tsunami deposits in Periya Kalapuwa Lagoon, eastern Sri Lanka. *Sediment Geol* 230:95–104
- Minoura K, Nakata T (1994) Discovery of an ancient tsunami deposit in coastal sequence of southwest Japan: verification of a large historic tsunami. *Island Arc* 3:66–72
- Mitra R, Naruse H, Abe T (2020) Estimation of tsunami characteristics from deposits: Inverse modeling using a deep-learning neural network. *J Geophys Res Earth Surf* 125:e2020JF005583. <https://doi.org/10.1029/2020JF005583>
- Mitra R, Naruse H, Fujino S (2021) Reconstruction of flow conditions from 2004 Indian Ocean tsunami deposits at the Phra Thong island using a deep neural network inverse model. *Nat Hazards Earth Syst Sci* 21:1667–1683. <https://doi.org/10.5194/nhess-21-1667-2021>
- Moore A, Goff J, McAdoo BG, Fritz HM, Gusman A, Kalligeris N, Kalsum K, Susanto A, Suteja D, Synolakis CE (2011) Sedimentary deposits from the 17 July 2006 Western Java Tsunami, Indonesia: Use of grain size analyses to assess tsunami flow depth, speed, and Traction carpet characteristics. *Pure Appl Geophys* 168:1951–1961. <https://doi.org/10.1007/s00024-011-0280-8>
- Mori N, Takahashi T, The 2011 Tohoku Earthquake Tsunami Joint Survey Group (2012) Nationwide post event survey and analysis of the 2011 Tohoku Earthquake Tsunami. *Coast Eng J* 54:1250001. <https://doi.org/10.1142/S0578563412500015>
- Morton RA, Gelfenbaum G, Jaffe BE (2007) Physical criteria for distinguishing sandy tsunami and storm deposits using modern examples. *Sediment Geol* 200:184–207
- Nakajima H, Koarai M (2011) Assessment of tsunami flood situation from the Great east Japan Earthquake. *Bull Geospat Inf Auth Jpn* 59:55–66
- Nanayama F, Satake K, Furukawa R, Shimokawa K, Atwater BF, Shigeno K, Yamaki S (2003) Unusually large earthquakes inferred from tsunami deposits along the Kuril trench. *Nature* 424:660–663. <https://doi.org/10.1038/nature01864>
- Nanayama F, Shigeno K (2006) Inflow and outflow facies from the 1993 tsunami in southwest Hokkaido. *Sediment Geol* 187:139–158
- Naruse H, Abe T (2017) Inverse tsunami flow modeling including nonequilibrium sediment transport, with application to deposits from the 2011 Tohoku-oki tsunami. *J Geophys Res Earth Surf* 122:2159–2182
- Naruse H, Arai K, Matsumoto D, Takahashi H, Yamashita S, Tanaka G, Murayama M (2012) Sedimentary features observed in the tsunami deposits at Rikuzentakata City. *Sediment Geol* 282:199–215
- Naruse H, Fujino S, Suphawajruksakul A, Jarupongsakul T (2010) Features and formation processes of multiple deposition layers from the 2004 Indian Ocean Tsunami at Ban Nam Kem, southern Thailand. *Island Arc* 19:399–411
- Ozawa S, Nishimura T, Suito H, Kobayashi T, Tobita M, Imakiire T (2011) Co-seismic and post-seismic slip of the 2011 magnitude-9 Tohoku-Oki earthquake. *Nature* 475:373–376. <https://doi.org/10.1038/nature10227>
- Paris R, Lavigne F, Wassmer P, Sartohadi J (2007) Coastal sedimentation associated with the December 26, 2004 tsunami in Lhok Nga, west Banda Aceh (Sumatra, Indonesia). *Mar Geol* 238:93–106. <https://doi.org/10.1016/j.margeo.2006.12.009>
- Pilarczyk JE, Horton BP, Witter RC, Vane CH, Chagué-Goff C, Goff J (2012) Sedimentary and foraminiferal evidence of the 2011 Tohoku-oki tsunami on the Sendai coastal plain, Japan. *Sediment Geol* 282:78–89
- Pilarczyk JE, Sawai Y, Namegaya Y, Tamura T, Tanigawa K, Matsumoto D, Shinozaki T, Fujiwara O, Shishikura M, Shimada Y, Dura T, Horton BP, Parnell AC, Vane CH (2021) A further source of Tokyo earthquakes and Pacific Ocean tsunamis. *Nat Geosci* 14:796–800. <https://doi.org/10.1038/s41561-021-00812-2>
- Richmond B, Szczuciński W, Chagué-Goff C, Goto K, Sugawara D, Witter R, Tappin DR, Jaffe B, Fujino S, Nishimura Y, Goff J (2012) Erosion, deposition and landscape change on the Sendai coastal plain, Japan, resulting from the March 11, 2011 Tohoku-oki tsunami. *Sediment Geol* 282:27–39
- Rubin CM, Horton BP, Sieh K, Pilarczyk JE, Daly P, Ismail N, Parnell AC (2017) Highly variable recurrence of tsunamis in the 7,400 years before the 2004 Indian Ocean tsunami. *Nat Commun* 8:16019. <https://doi.org/10.1038/ncomms16019>
- Sawai Y (2012) Study on paleotsunami deposits in geologic stratum. *J Geol Soc Jpn* 118:535–558. <https://doi.org/10.5575/geosoc.2012.0063>. ((in Japanese))
- Sawai Y, Jankaew K, Martin ME, Prendergast A, Choowong M, Charoentitirat T (2009a) Diatom assemblages in tsunami deposits associated with the 2004 Indian Ocean tsunami at Phra Thong Island, Thailand. *Mar Micropaleontol* 73:70–79. <https://doi.org/10.1016/j.marmicro.2009.07.003>
- Sawai Y, Kamataki T, Shishikura M, Nasu H, Okamura Y, Satake K, Thomson KH, Matsumoto D, Fujii Y, Komatsubara J, Aung TT (2009b) Aperiodic recurrence of geologically recorded tsunamis during the past 5500 years in eastern Hokkaido, Japan. *J Geophys Res Solid Earth* 114:B01319. <https://doi.org/10.1029/2007JB005503>
- Sawai Y, Namegaya Y, Okamura Y, Satake K, Shishikura M (2012) Challenges of anticipating the 2011 Tohoku earthquake and tsunami using coastal geology. *Geophys Res Lett* 39:L21309. <https://doi.org/10.1029/2012GL053692>
- Sawai Y, Namegaya Y, Tamura T, Nakashima R, Tanigawa K (2015) Shorter intervals between great earthquakes near Sendai: Scour ponds and a sand layer attributable to AD 1454 overwash. *Geophys Res Lett* 42:4795–4800. <https://doi.org/10.1002/2015GL064167>
- Shimada Y, Fujino S, Sawai Y, Tanigawa T, Matsumoto D, Momohara A, Saito-Kato M, Yamada M, Hirayama E, Suzuki T, Chagué C (2019) Geological record of prehistoric tsunamis in Mugi town, facing the Nankai Trough, western Japan. *Prog Earth Planet Sci* 6:33. <https://doi.org/10.1186/s40645-019-0279-9>
- Sohn YK (1997) On traction-carpet sedimentation. *J Sediment Res* 67:502–509

- Spiske M, Tang H, Bahlburg H (2020) Post-depositional alteration of onshore tsunami deposits—implications for the reconstruction of past events. *Earth-Sci Rev*. <https://doi.org/10.1016/j.earscirev.2019.103068>
- Sugawara D, Imamura F, Matsumoto H, Goto K, Minoura K (2010) Quantitative reconstruction of a paleo-tsunami: field survey of Jōgan tsunami and paleotopography. *DCRC Tsunami Eng* 27:103–132 ((in Japanese))
- Sugawara D, Imamura F, Goto K, Matsumoto H, Minoura K (2013) The 2011 Tohoku-oki Earthquake Tsunami: similarities and differences to the 869 Jogan Tsunami on the Sendai Plain. *Pure Appl Geophys* 170:831–843. <https://doi.org/10.1007/s00024-012-0460-1>
- Szczuciński W, Kokociński M, Rzeszewski M, Chagué-Goff C, Cachão M, Goto K, Sugawara D (2012) Sediment sources and sedimentation processes of 2011 Tohoku-oki tsunami deposits on the Sendai Plain, Japan—Insights from diatoms, nannoliths and grain size distribution. *Sediment Geol* 282:40–56
- Takashimizu Y, Urabe A, Suzuki K, Sato Y (2012) Deposition by the 2011 Tohoku-oki tsunami on coastal lowland controlled by beach ridges near Sendai, Japan. *Sediment Geol* 282:124–141
- Tamura T, Masuda F (2004) Inner shelf to shoreface depositional sequence in the Sendai coastal prism, Pacific coast of northeastern Japan: spatial and temporal growth patterns in relation to Holocene relative sea-level change. *J Asian Earth Sci* 23:567–576. <https://doi.org/10.1016/j.jseas.2003.09.002>
- Tang H, Wang J, Weiss R, Xiao H (2017) TSUFLIND-EnKF: inversion of tsunami flow depth and flow speed from deposits with quantified uncertainties. *Mar Geol* 396:16–25
- Tang H, Weiss R (2015) A model for tsunami flow inversion from deposits (TSUFLIND). *Mar Geol* 99:10143–10162
- Tanigawa K, Sawai Y, Namegaya Y (2018) Diatom assemblages within tsunami deposit from the Tohoku-oki earthquake along the Misawa coast, Aomori Prefecture, northern Japan. *Mar Geol* 396:6–15. <https://doi.org/10.1016/j.margeo.2016.11.016>
- The 2011 Tohoku Earthquake Tsunami Joint Survey Group (2011) Nationwide field survey of the 2011 off the Pacific coast of Tohoku Earthquake Tsunami. *J Jpn Soc Civ Eng B2* 67:63–66
- Tuttle MP, Ruffman A, Anderson T, Jeter H (2004) Distinguishing tsunami from storm deposits in eastern North America: The 1929 Grand Banks tsunami versus the 1991 Halloween storm. *Seismol Res Lett* 75:117–131

Publisher's Note

Springer Nature remains neutral with regard to jurisdictional claims in published maps and institutional affiliations.

Submit your manuscript to a SpringerOpen[®] journal and benefit from:

- Convenient online submission
- Rigorous peer review
- Open access: articles freely available online
- High visibility within the field
- Retaining the copyright to your article

Submit your next manuscript at ► [springeropen.com](https://www.springeropen.com)
